



# Effects of H<sub>2</sub> on microstructures of Cr<sub>2</sub>O<sub>3</sub> scales grown in water vapour and consequences for breakaway

Thuan Dinh Nguyen, Jianqiang Zhang\*, David J. Young

School of Materials Science and Engineering, University of New South Wales, Sydney, NSW 2052, Australia

## ARTICLE INFO

### Keywords:

Steels

Water vapour

Hydrogen

High temperature corrosion

## ABSTRACT

Model alloy, Fe-20Cr (wt%), was exposed in Ar-(5, 20)H<sub>2</sub>O, Ar-(5, 20)H<sub>2</sub>O-5H<sub>2</sub> and Ar-20O<sub>2</sub> (vol%) at 750 and 850 °C. The alloy formed Cr<sub>2</sub>O<sub>3</sub> scales plus Fe-rich oxide nodules in H<sub>2</sub>O-containing gases, but a Cr<sub>2</sub>O<sub>3</sub> scale in Ar-20O<sub>2</sub> at 750 °C. The alloy formed an outer (Cr,Fe)-rich oxide layer and an inner, porous Cr<sub>2</sub>O<sub>3</sub> layer in Ar-5H<sub>2</sub>O-5H<sub>2</sub>, whereas a dense Cr<sub>2</sub>O<sub>3</sub> scale grew in Ar-5H<sub>2</sub>O at 850 °C. Application of Wagner's theory successfully differentiated effects of oxide grain sizes and oxygen partial pressures of gases on scaling rates. Chemically inert SiO<sub>2</sub> markers showed that Cr<sub>2</sub>O<sub>3</sub> scales grew by outward metal diffusion.

## 1. Introduction

Combustion of coal, oil, and natural gases in power plants releases a flue gas rich in CO<sub>2</sub> and water vapour. New combustion technologies are being developed to use hydrogen instead of hydrocarbons to produce a H<sub>2</sub>O-rich flue gas, consequently reducing greenhouse gas (CO<sub>2</sub>) emission. Water vapour is clearly present in almost all flue gases, sometimes with a small amount of H<sub>2</sub>. For this reason, steam oxidation resistance can be an important factor when selecting alloys for high temperature applications.

Chromia-forming stainless steels used in heat exchangers rely on formation and maintenance of a slow growing Cr<sub>2</sub>O<sub>3</sub> scale for corrosion resistance. This Cr<sub>2</sub>O<sub>3</sub> scale provides effective protection for oxidation in dry air/O<sub>2</sub> [1–4] but can fail to do so in water vapour [3–6]. Addition of H<sub>2</sub> to water vapour significantly reduced weight uptakes on Fe-20Cr-0.06Al (all alloy compositions in wt%) at 900 and 1050 °C by forming a thin Cr<sub>2</sub>O<sub>3</sub> scale [5]. At a fixed water vapour level, increasing H<sub>2</sub> levels slightly decreased growth rates of Fe-rich oxide scales on 304 L steel at 600 °C [7]. Although high temperature oxidation in H<sub>2</sub>O/H<sub>2</sub>O-H<sub>2</sub> has been studied extensively for commercial steels and pure chromium [8–10], knowledge of the effects of H<sub>2</sub> on microstructures and growth of chromia scales formed in water vapour at intermediate temperatures (650–900 °C) is still limited.

In this work, a model Fe-20Cr alloy was exposed to five gas mixtures Ar-(5, 20)H<sub>2</sub>O, Ar-(5, 20)H<sub>2</sub>O-5H<sub>2</sub> and Ar-20O<sub>2</sub> (vol%) at 750 and 850 °C. The 20 wt% Cr concentration was chosen because it is used in commercial steels like 441 and Crofer 22 APU. The aim was to

investigate effects of temperatures and gas compositions on failure and microstructures of chromia scales in H<sub>2</sub>O/H<sub>2</sub>O-H<sub>2</sub>. The growth mechanism of Cr<sub>2</sub>O<sub>3</sub> scales in Ar-5H<sub>2</sub>O and Ar-5H<sub>2</sub>O-5H<sub>2</sub> was investigated using inert SiO<sub>2</sub> marker tests. Penetration of hydrogen through Cr<sub>2</sub>O<sub>3</sub> scales was studied by replacing H<sub>2</sub>O with D<sub>2</sub>O.

## 2. Materials and experiments

A model Fe-20Cr alloy (wt%) was prepared by arc melting pure metals Fe (99.98 %, Sigma Aldrich) and Cr (99.995 %, Sigma Aldrich) under a protective Ar-5H<sub>2</sub> (volume %) gas atmosphere, using a non-consumable electrode. The resulting button was annealed at 1000 °C for 70 h in a flowing Ar-5H<sub>2</sub> gas for homogenization. The alloy grain sizes after annealing were 3 ± 2 mm. Rectangular alloy coupons (1 ± 0.1) × (8 ± 1) × (8 ± 1) mm in size were surface ground to a 1200-grit finish, electropolished to remove deformed surface material, and ultrasonically cleaned in alcohol prior to reaction. The alloy composition was checked by scanning electron microscopy (SEM)/energy dispersive X-ray spectrometer (EDX) (detection limit of 0.1 wt%) and found to be within 0.2 % of the nominal concentrations for Cr.

Alloy specimens were reacted at 750 and 850 °C in flowing Ar-(5, 20)H<sub>2</sub>O, Ar-(5, 20)H<sub>2</sub>O-5H<sub>2</sub> and Ar-20O<sub>2</sub> mixtures (volume %) with a total pressure of 1 atm for 70 h using a TGA (Thermo Gravimetric Analyser) equipped with a CI Precision microbalance with an accuracy of 0.1 µg. Linear gas flow rates were 0.8 cm/s at 750 °C and 0.9 cm/s at 850 °C. Equilibrium partial pressures of the reaction gases are summarised in Table 1. The oxygen purity was 99.999 %.

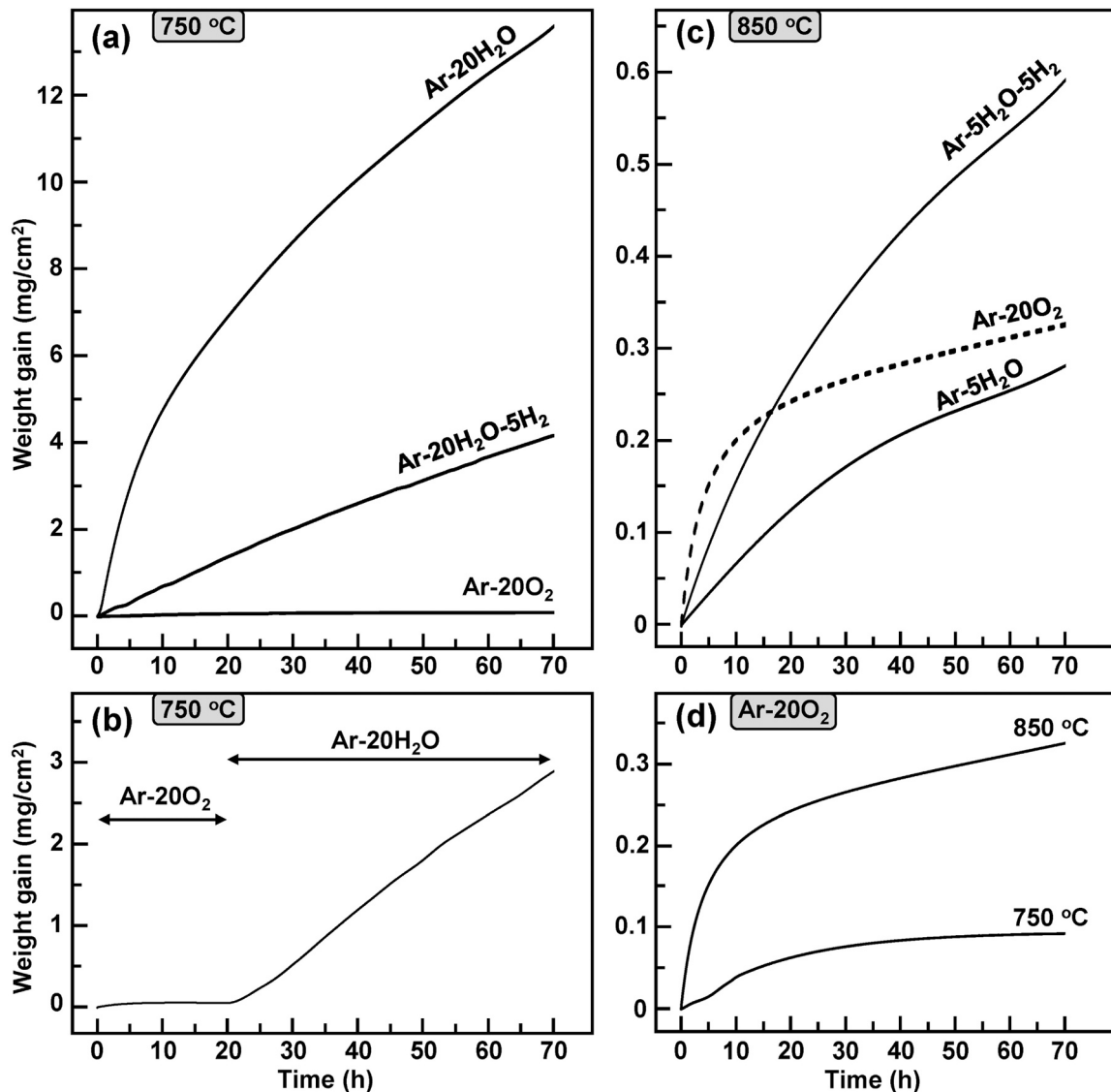
\* Corresponding author.

E-mail address: [j.q.zhang@unsw.edu.au](mailto:j.q.zhang@unsw.edu.au) (J. Zhang).

**Table 1**

Equilibrium partial pressures (atm) of gas compositions at 750 and 850 °C calculated by Factsgage [11].

Species	Pressure (atm)				
	750 °C		850 °C		
	Ar-20 O <sub>2</sub>	Ar-20 H <sub>2</sub> O	Ar-20 H <sub>2</sub> O-5 H <sub>2</sub>	Ar-5 H <sub>2</sub> O	Ar-5 H <sub>2</sub> O-5 H <sub>2</sub>
O <sub>2</sub>	0.2	$6.5 \times 10^{-8}$	$4.6 \times 10^{-19}$	$1.5 \times 10^{-7}$	$5.2 \times 10^{-18}$
H <sub>2</sub>		$1.3 \times 10^{-7}$	0.05	$3 \times 10^{-7}$	0.05

**Fig. 1.** Weight gain kinetics of Fe-20Cr reacted in different gases at: (a) 750 °C, (b) two stages at 750 °C (20 h in Ar-20 O<sub>2</sub> then 50 h in Ar-20 H<sub>2</sub>O), (c) 850 °C, and (d) 750 and 850 °C in Ar-20 O<sub>2</sub>.

Corroded samples were characterized by Raman spectroscopy (Renishaw, 532 nm diode laser), scanning electron microscopy (Hitachi S3400) with an energy dispersive X-ray spectrometer (Bruker) and transmission electron microscopy (TEM, JEOL JEM-F200). The TEM samples were prepared using a focused ion beam system (FIB, FEI Helios G4 PFIB) with a maximum accelerating voltage of 30 kV.

An inert marker test was performed to study growth mechanism of Cr<sub>2</sub>O<sub>3</sub> scales in Ar-5H<sub>2</sub>O-(5H<sub>2</sub>) at 850 °C. The sample surface was sprayed with fine, amorphous SiO<sub>2</sub> powder (< 0.2 μm) and then oxidised for 24 h. Analysis by TEM/EDX was used to determine the distribution of SiO<sub>2</sub> markers in the Cr<sub>2</sub>O<sub>3</sub> scale.

To investigate the location of hydrogen within chromia, another higher Cr concentration model alloy, Fe-30Cr, was selected to ensure that a uniform Cr<sub>2</sub>O<sub>3</sub> scale forms in Ar-10H<sub>2</sub>O. A reaction temperature of 650 °C was used to ensure that the Cr<sub>2</sub>O<sub>3</sub> scale thickness was not too thick for depth profiling analysis. The Fe-30Cr alloy was exposed to Ar-10H<sub>2</sub>O and Ar-10D<sub>2</sub>O at 650 °C. A two-stage experiment was carried out for 30 min in Ar-10H<sub>2</sub>O and then 30 min in Ar-10D<sub>2</sub>O. Distribution of hydrogen and deuterium in Cr<sub>2</sub>O<sub>3</sub> scales was analysed by ToF-SIMS (TOF.SIMS5-IONTOF). A sputter area of 300 × 300 μm<sup>2</sup> was etched by a Cs<sup>+</sup> ion beam (1 keV, 70.9 nA). A Bi<sup>+</sup> ion beam (30 keV, 2.6 pA) was used to produce negative ion profiles, using an analysis area of 100 ×

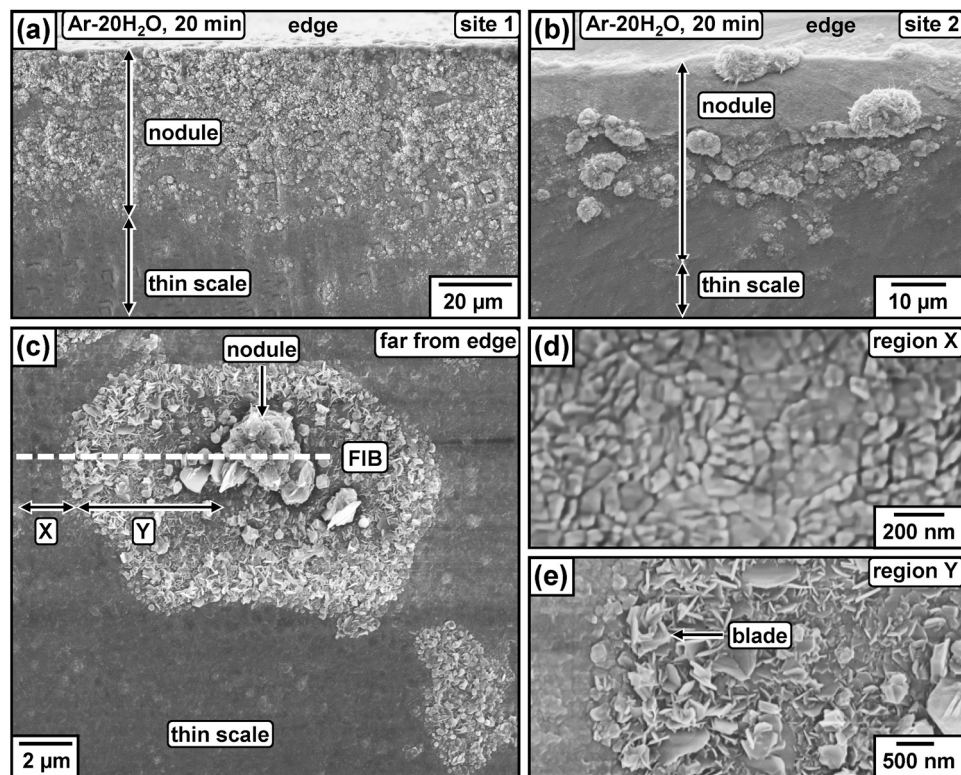


**Fig. 2.** SE-SEM (Secondary Electron-SEM) top views of Fe-20Cr oxidized at 750 °C for 20 min in Ar-20 H<sub>2</sub>O: sample edges at (a) site 1 and (b) site 2, (c) region far from edge showing location of FIB milling, high magnification images of (d) region X and (e) region Y in (c).

100 μm<sup>2</sup>. The samples were loaded into an analysis chamber, which was pumped for two days until the base pressure was less than  $5 \times 10^{-10}$  mbar before starting measurements.

### 3. Results

Weight gains of Fe-20Cr in different gases are shown in Fig. 1. Weight uptakes in Ar-20H<sub>2</sub>O-(5H<sub>2</sub>) were much greater than that in Ar-20O<sub>2</sub> and increased significantly with time at 750 °C. The addition of H<sub>2</sub> to Ar-20H<sub>2</sub>O markedly reduced the weight uptake at 750 °C. In the two-stage experiment at 750 °C (Fig. 1b), weight uptake was small for the first 20 h in Ar-20O<sub>2</sub>, but increased rapidly when the gas was changed to Ar-20H<sub>2</sub>O. Weight uptake at 850 °C in Ar-20O<sub>2</sub> was smaller than that in Ar-5H<sub>2</sub>O-5H<sub>2</sub> but greater than that in Ar-5 H<sub>2</sub>O (Fig. 1c). Weight uptakes in Ar-20O<sub>2</sub> increased with reaction temperature (Fig. 1d).

#### 3.1. Reaction at 750 °C

##### 3.1.1. Initial reaction stage in Ar-20H<sub>2</sub>O

Surface views of Fe-20Cr oxidised in Ar-20H<sub>2</sub>O for 20 min are shown in Fig. 2. The alloy formed a thin scale and nodules distributed mainly along samples edges (Fig. 2a, b). A few nodules were found on regions far from the sample edges (Fig. 2c). The region Y surrounding a nodule contained oxide blades on the surface (Fig. 2c, e), whilst only fine grains had formed in the more distant region X (Fig. 2c, d). The measured surface area fraction of nodules was about 2 %. The nodule and surrounding regions X, Y in Fig. 2c were milled by FIB for TEM analysis.

A BF-STEM (Bright Field-Scanning TEM) cross-section of the coarse nodule in Fig. 2c is shown in Fig. 3a. Analysis by EDX (Fig. 3b, c) revealed the nodule to consist of an outer Fe<sub>2</sub>O<sub>3</sub> layer, an intermediate (Cr,Fe)-rich oxide layer, and an inner Cr<sub>2</sub>O<sub>3</sub> layer. Internal oxidation zones (IOZs) beneath the nodule contained Cr-rich oxide precipitates

(Fig. 3a, b). A finer nodule without any IOZ was observed next to the coarse nodule (Fig. 3a, b).

A BF-STEM cross-section of the thin scale on regions X and Y in Fig. 2c is shown in Fig. 4a. Thicknesses of the scales on regions X and Y are 60 and 150 nm, respectively. Analysis by EDX (Fig. 4b-d) indicated the scale on region Y to be Cr<sub>2</sub>O<sub>3</sub>. The scale on region X was made up of an outer (Fe, Cr)-rich oxide layer and an inner Cr<sub>2</sub>O<sub>3</sub> layer (Fig. 4e-g).

##### 3.1.2. Thick scales formed in Ar-20H<sub>2</sub>O-(5H<sub>2</sub>)

The Fe-20Cr alloy had formed a mixture of Cr<sub>2</sub>O<sub>3</sub> scale and Fe-rich oxide nodules in H<sub>2</sub>O-containing gases after 70 h exposure at 750 °C. Surface area fractions of Fe-rich oxide nodules formed in Ar-20H<sub>2</sub>O, Ar-20H<sub>2</sub>O-5H<sub>2</sub>, and after the two-stage reaction (O<sub>2</sub> then H<sub>2</sub>O) were 36, 14, and 14 %, respectively.

Optical microscope cross-sections of Fe-rich oxide nodules formed at 750 °C in the two water vapour-bearing gases are shown in Fig. 5. Analyses by Raman (Fig. 5d) [12,13] and SEM/EDX (Fig. 5e) indicated the nodule in Ar-20H<sub>2</sub>O to consist of an outer Fe<sub>2</sub>O<sub>3</sub> layer (~ 13 μm), an intermediate Fe<sub>3</sub>O<sub>4</sub> layer (~ 45 μm), and an inner (Fe<sub>3</sub>O<sub>4</sub>+FeCr<sub>2</sub>O<sub>4</sub>) layer (~ 50 μm). The nodule in Ar-20H<sub>2</sub>O-5H<sub>2</sub> was made up of an outer Fe<sub>3</sub>O<sub>4</sub> layer (~ 30 μm), and an inner (Fe<sub>3</sub>O<sub>4</sub>+FeCr<sub>2</sub>O<sub>4</sub>) layer (~ 31 μm). Pores were observed mainly at the interface between the Fe<sub>3</sub>O<sub>4</sub> and (Fe<sub>3</sub>O<sub>4</sub>+FeCr<sub>2</sub>O<sub>4</sub>) layers for the nodule formed in Ar-20H<sub>2</sub>O-5H<sub>2</sub> (Fig. 5c) but throughout the Fe<sub>3</sub>O<sub>4</sub> layer of the nodule in Ar-20H<sub>2</sub>O (Fig. 5b).

A small nodule without an inner layer (Fig. 5a) was analysed by SEM/EDX (Fig. 6). No Cr-rich oxide layer at the nodule-alloy interface is visible at these magnifications (Fig. 6b, d). An internal oxidation zone (IOZ) containing Cr-rich oxide precipitates formed beneath the nodule (Fig. 6c, e). The nodule-alloy interface was analysed further by TEM/EDX (Fig. 7), revealing a thin Cr-rich oxide layer (~ 48 nm).

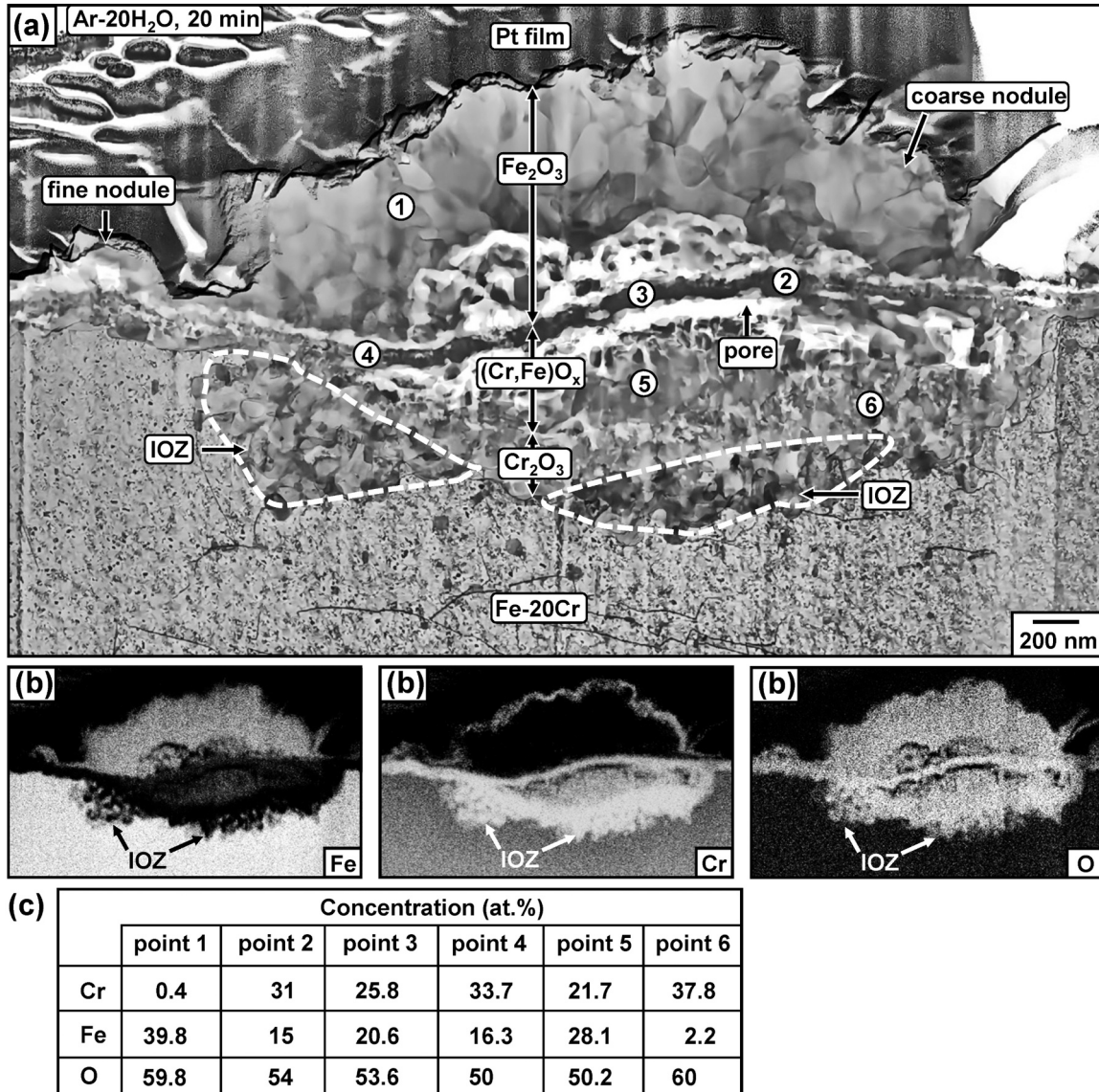
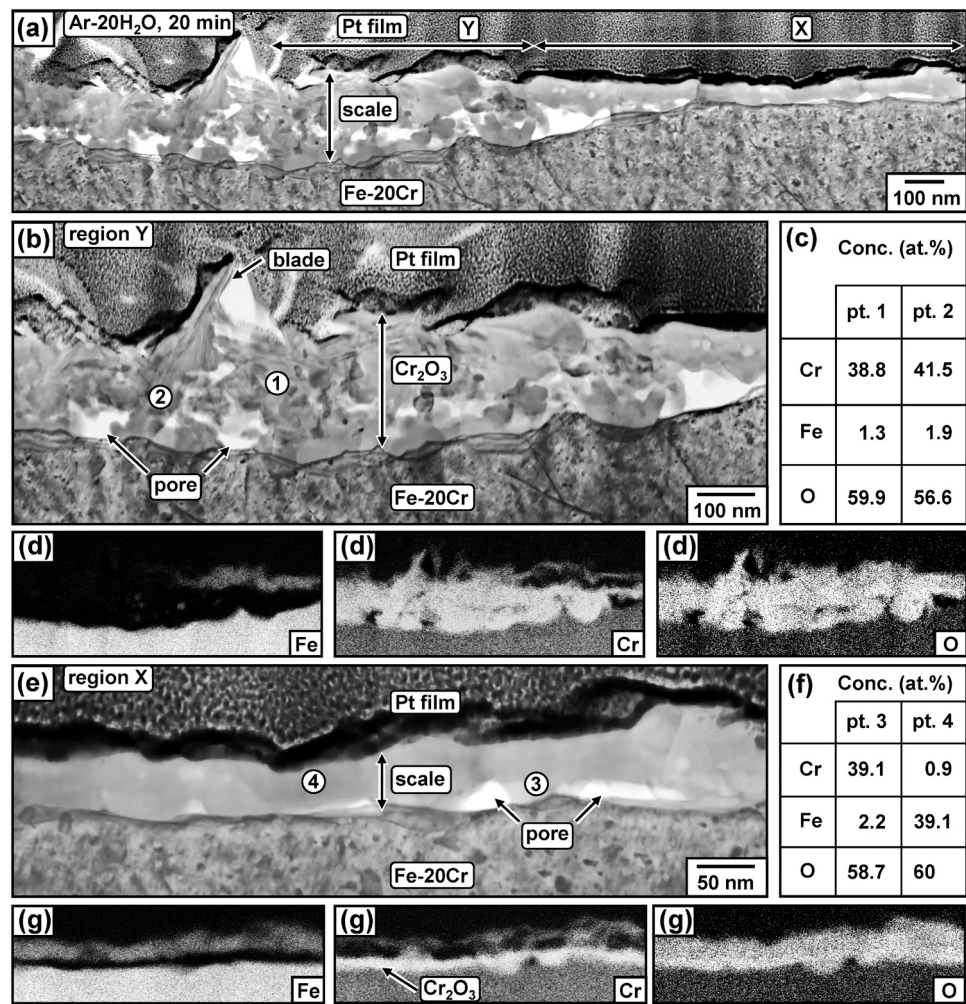


Fig. 3. Fe-20Cr oxidized for 20 min in Ar-20 H<sub>2</sub>O at 750 °C: (a) BF-STEM cross-section of the nodule in Fig. 2c, (b) EDX mapping of (a), and (c) EDX concentrations of points 1–6 in (a).



**Fig. 4.** Fe-20Cr oxidized for 20 min in Ar-20 H<sub>2</sub>O at 750 °C: (a) BF-STEM cross-section of the regions X and Y (thin scale) in Fig. 2c, (b) high magnification image of region Y in (a), (c) EDX concentrations of points 1–2 and (d) mapping of (b), (e) high magnification image of region X in (a), (f) EDX concentrations of points 3–4 and (g) mapping of (e).

### 3.1.3. Reaction in Ar-20O<sub>2</sub> and two-stage reaction

Analysis by TEM/EDX (Fig. 10) shows that Fe-20Cr alloy formed a uniform Cr<sub>2</sub>O<sub>3</sub> scale in Ar-20O<sub>2</sub> after 70 h exposure at 750 °C (Fig. 8a). Analyses by TEM/EDX (Fig. 10) and Raman (not shown) show that the two-stage reaction sample formed a mixture of Cr<sub>2</sub>O<sub>3</sub> scales and Fe-rich oxide nodules (Fig. 8b). The nodule in Fig. 8c was made up of an outer Fe<sub>2</sub>O<sub>3</sub> layer (~ 8 µm), an intermediate Fe<sub>3</sub>O<sub>4</sub> layer (~ 20 µm), and an inner (Fe<sub>3</sub>O<sub>4</sub>+FeCr<sub>2</sub>O<sub>4</sub>) layer (~ 24 µm). Pores were observed mainly in the Fe<sub>3</sub>O<sub>4</sub> layer and at the scale-alloy interface.

### 3.1.4. Morphologies of Cr<sub>2</sub>O<sub>3</sub> scales formed in different gases

Surface views and cross-sections of the Cr<sub>2</sub>O<sub>3</sub> scale regions are shown in Figs. 9 and 10. Reaction in Ar-20 O<sub>2</sub> resulted in chromia grains coarser than those in other gases (Table 2). Fine and coarse grains were observed on the Cr<sub>2</sub>O<sub>3</sub> scale surface of the two-stage reaction sample (Figs. 9d, 10e). The Cr<sub>2</sub>O<sub>3</sub> scale formed in Ar-20H<sub>2</sub>O-5H<sub>2</sub> consisted of an outer, fine-grained layer (layer 1) and an inner, coarse-grained layer (layer 2) (Fig. 10f). A small amount of Fe was detected in all Cr<sub>2</sub>O<sub>3</sub> scales (Fig. 10g-k), whilst Si was observed only in Cr<sub>2</sub>O<sub>3</sub> scales formed in Ar-20H<sub>2</sub>O (Fig. 10h) and Ar-20H<sub>2</sub>O-5H<sub>2</sub> in the outer layer (Fig. 10i). Deionised liquid water used to produce water vapour contained trace amounts of Si-bearing compounds [14,15]. For this reason, silicon was sometimes detected in chromia scales formed in water vapour.

### 3.2. Reaction at 850 °C

#### 3.2.1. Reaction in Ar-5H<sub>2</sub>O

The Fe-20Cr alloy formed a thin, uniform Cr<sub>2</sub>O<sub>3</sub> scale in Ar-5 H<sub>2</sub>O at 850 °C (Figs. 11, 12). The Cr<sub>2</sub>O<sub>3</sub> scale (about 1.8 µm thick) was dense and made up of equiaxed and columnar grains. The equiaxed grains were observed mainly near the scale surface and at the scale-alloy interface, whilst columnar grains made up most of the scale interior.

#### 3.2.2. Reaction in Ar-5H<sub>2</sub>O-5H<sub>2</sub>

After reaction in Ar-5H<sub>2</sub>O-5H<sub>2</sub>, the alloy surface was covered by Fe-rich oxide (surface area fraction about 38 %) and Cr-rich oxide regions (Fig. 13).

Analysis by TEM/EDX (Fig. 14) of the Cr-rich oxide region seen in Fig. 13b confirmed the Cr<sub>2</sub>O<sub>3</sub> scale (about 2.5 µm thick). The BF-STEM (Fig. 14d) and Dark Field (DF)-STEM (Fig. 14e) images confirmed the formation of numerous small, random pores in the Cr<sub>2</sub>O<sub>3</sub> scale by highlighting pores in bright and dark contrasts, respectively. The pores were observed along columnar oxide grain boundaries and inside grains. The volume fraction of pores was about 6 %.

A BF-STEM cross-section of the Fe-rich oxide region imaged in Fig. 13b is shown in Fig. 15. The scale was analysed by TEM/EDX and found to consist of an outer, (Fe,Cr)-rich oxide layer (about 0.6 µm

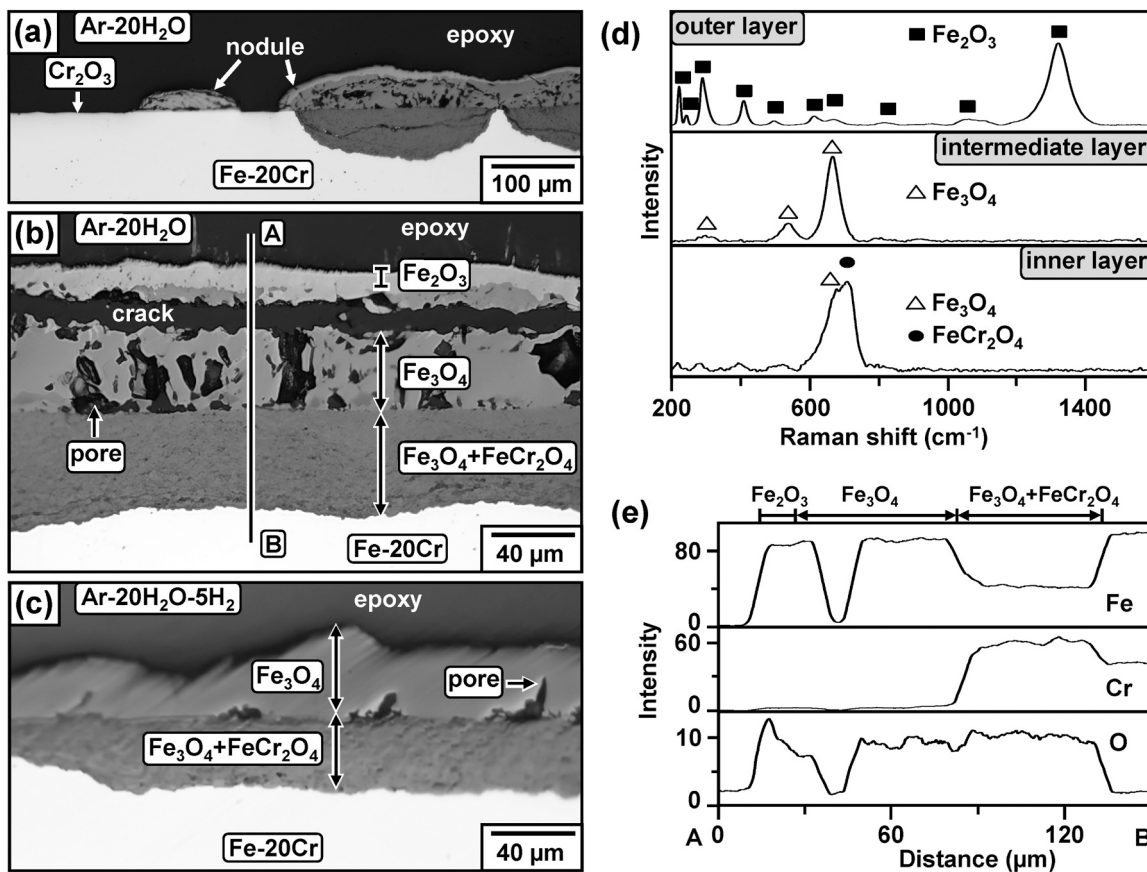


**Fig. 5.** Cross-sections of Fe-20Cr oxidized for 70 h at 750 °C: (a) low magnification image (Ar-20 H<sub>2</sub>O), (b) high magnification image of a nodule in (a), (c) high magnification image of a nodule (Ar-20 H<sub>2</sub>O-5 H<sub>2</sub>), (d) Raman spectra of three scale layers and (e) SEM/EDX line profiles along A-B in (b).

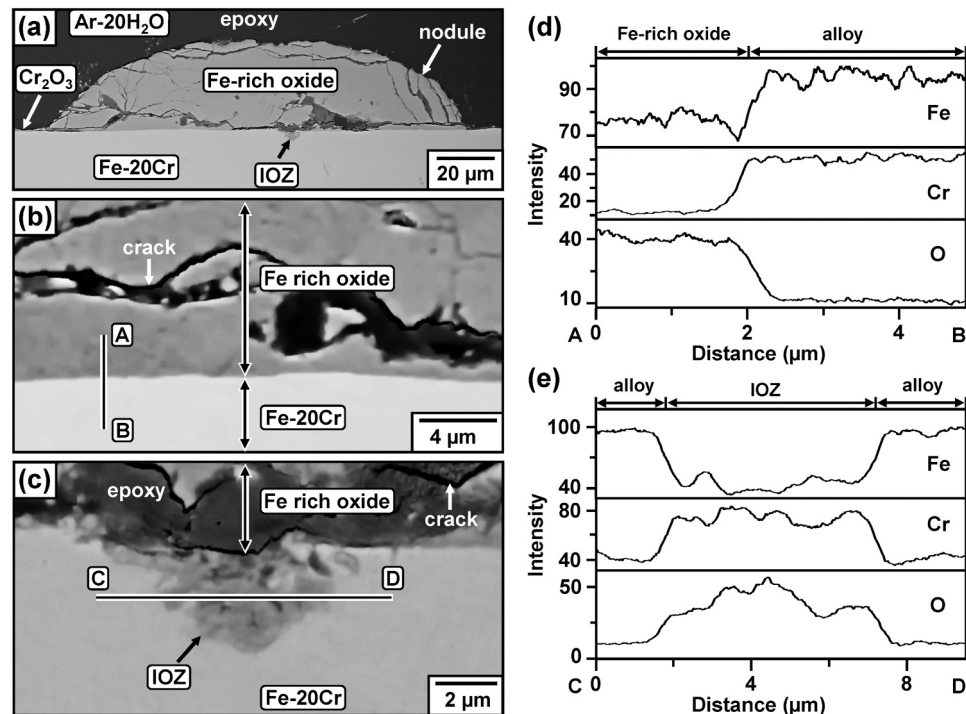


**Fig. 6.** Fe-20Cr oxidized for 70 h in Ar-20H<sub>2</sub>O at 750 °C: (a) low magnification BSE-SEM image of a small Fe-rich nodule in Fig. 5a, (b) high magnification image of the nodule-alloy interface in (a), (c) high magnification image of IOZ in (a), EDX line profiles along (d) A-B in (b) and (e) C-D in (c).

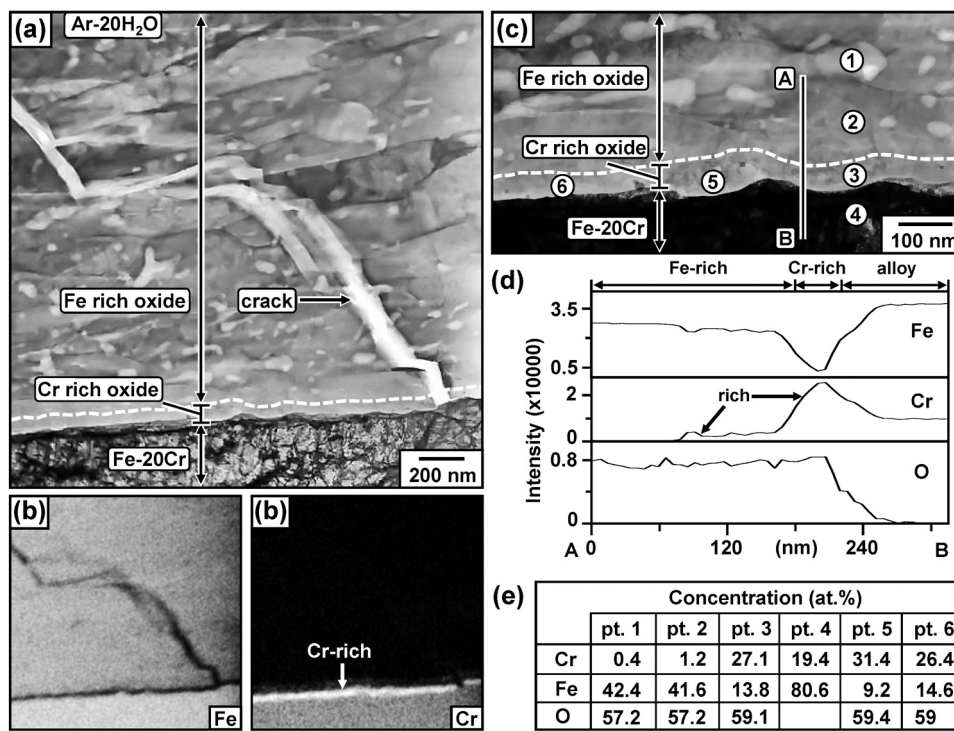


**Fig. 7.** Fe-20Cr oxidized for 70 h in Ar-20 H<sub>2</sub>O at 750 °C: (a) BF-STEM cross-section of the nodule-alloy interface in Fig. 6b, (b) EDX mapping of (a), (c) high magnification image of the nodule-alloy interface in (a), (d) EDX line profiles along A-B in (c), and (e) EDX concentrations of points 1–4 in (c).

thick) and an inner Cr<sub>2</sub>O<sub>3</sub> layer (about 2.7 µm thick) (Fig. 15b, c). Fine pores were observed throughout the scale. The volume fraction of pores was about 6 %. Chromia scales formed in Ar-5H<sub>2</sub>O-5H<sub>2</sub> at 850 °C consisted of mainly columnar grains and some randomly distributed equiaxed grains.

### 3.2.3. Reaction in Ar-20O<sub>2</sub>

The Fe-20Cr alloy formed a uniform but convoluted Cr<sub>2</sub>O<sub>3</sub> scale after exposure in Ar-20O<sub>2</sub> at 850 °C for 70 h (Figs. 16, 17). The Cr<sub>2</sub>O<sub>3</sub> scale (about 1.9 µm thick) was made up of fine and coarse, equiaxed grains. The coarse Cr<sub>2</sub>O<sub>3</sub> grains were located near the scale surface, whilst the fine ones were distributed mainly at the scale-alloy interface. The fine porosity seen in Cr<sub>2</sub>O<sub>3</sub> grown in 5H<sub>2</sub>O-5H<sub>2</sub> (Figs. 14, 15) was not present after reaction in O<sub>2</sub>.

Thicknesses of Cr<sub>2</sub>O<sub>3</sub> scales formed in different gases at 750 and 850 °C are shown in Tables 2 and 3. The Cr<sub>2</sub>O<sub>3</sub> scale formed in Ar-20O<sub>2</sub> was thicker than those in Ar-20H<sub>2</sub>O-(5H<sub>2</sub>) at 750 °C. The Cr<sub>2</sub>O<sub>3</sub> scales formed in H<sub>2</sub>O were thinner than those in H<sub>2</sub>O-H<sub>2</sub> at both 750 and 850 °C.

### 3.3. Inert SiO<sub>2</sub> marker tests at 850 °C

A BF-STEM cross-section of the inert SiO<sub>2</sub> marker test after reaction in Ar-5H<sub>2</sub>O at 850 °C for 24 h is shown in Fig. 18. The Cr<sub>2</sub>O<sub>3</sub> scale (1600 ± 200 nm) was dense and consisted of an outer, fine grained layer (layer 1) and an inner, fine-coarse grained layer (layer 2). Analysis by TEM/EDX revealed the SiO<sub>2</sub> marker near the scale-alloy interface (Fig. 18a, b, c). The SiO<sub>2</sub> grains along Cr<sub>2</sub>O<sub>3</sub> grain boundaries reduced coalescence and growth, resulting in finer, equiaxed Cr<sub>2</sub>O<sub>3</sub> grains in regions containing SiO<sub>2</sub> grains (Fig. 18). The Cr<sub>2</sub>O<sub>3</sub> scale with markers grown for 24 h consisted of mainly fine, equiaxed grains (Fig. 18), whilst that without markers formed for 70 h was made up of mainly coarser, columnar grains (Fig. 12). However, as seen in Fig. 18, regions of the scale where no markers are visible had developed columnar grains as well as fine-grained oxide.

A BF-STEM cross-section of the inert SiO<sub>2</sub> marker test in Ar-5H<sub>2</sub>O-5H<sub>2</sub> at 850 °C for 24 h is shown in Fig. 19. Analyses by TEM/EDX (Fig. 19b, c) confirmed that the scale (1700 ± 200 nm) was made up of an outer (Fe,Cr)-rich oxide layer and an inner Cr<sub>2</sub>O<sub>3</sub> layer which was mostly fine grained, but coarse grained near the alloy interface. Fine pores formed throughout the scale. The SiO<sub>2</sub> marker was found near the scale-alloy interface (Fig. 19a, b, d). The volume fraction of pores was about 6 %. The scale with SiO<sub>2</sub> markers (24 h) (Fig. 19) consisted of mainly fine grains, while that without markers grown for 70 h was made up mostly of coarser, columnar grains (Figs. 14, 15).

The Cr<sub>2</sub>O<sub>3</sub> scales formed at 850 °C (Figs. 12, 14, 15, 17–19) were made up of both fine and coarse grains. Therefore, only maximum grain sizes are shown in Table 3. Chromia grains grew with increasing reaction time in Ar-5H<sub>2</sub>O-(5H<sub>2</sub>).

### 3.4. ToF-SIMS analysis of Cr<sub>2</sub>O<sub>3</sub> scales formed at 650 °C

A uniform Cr<sub>2</sub>O<sub>3</sub> scale formed on Fe-30Cr alloy in pure O<sub>2</sub> for 30 min was used to study deuterium and hydrogen backgrounds in the absence of H-bearing species. The ToF-SIMS depth profiles of the Cr<sub>2</sub>O<sub>3</sub> scale in Fig. 20a showed a significant hydrogen concentration at the outermost scale surface which reduced sharply to the scale interior. This hydrogen detection is attributed to surface contamination. Deuterium signals of Cr<sub>2</sub>O<sub>3</sub> scales formed in O<sub>2</sub> (Fig. 20a) and Ar-10H<sub>2</sub>O (Fig. 20b) were weak and can be neglected.

The hydrogen depth profiles of Cr<sub>2</sub>O<sub>3</sub> scales formed on Fe-30Cr in Ar-10H<sub>2</sub>O (Fig. 20b), Ar-10D<sub>2</sub>O (Fig. 21) and two stages (Fig. 22) were similar to that formed in pure O<sub>2</sub> (Fig. 20a), but yielded weak hydrogen signals in the scale. These are regarded as unreliable results, as readily attributable to contamination (Fig. 20a) as to any other cause.

The experiments with Ar-10D<sub>2</sub>O (Figs. 21, 22) were carried out to allow ToF-SIMS detection for the hydrogen isotope, unaffected by atmospheric or instrumental contamination. As is seen, the D concentration was high at the outermost scale surface and near the scale-alloy interface. No deuterium was detected in the underlying alloy.

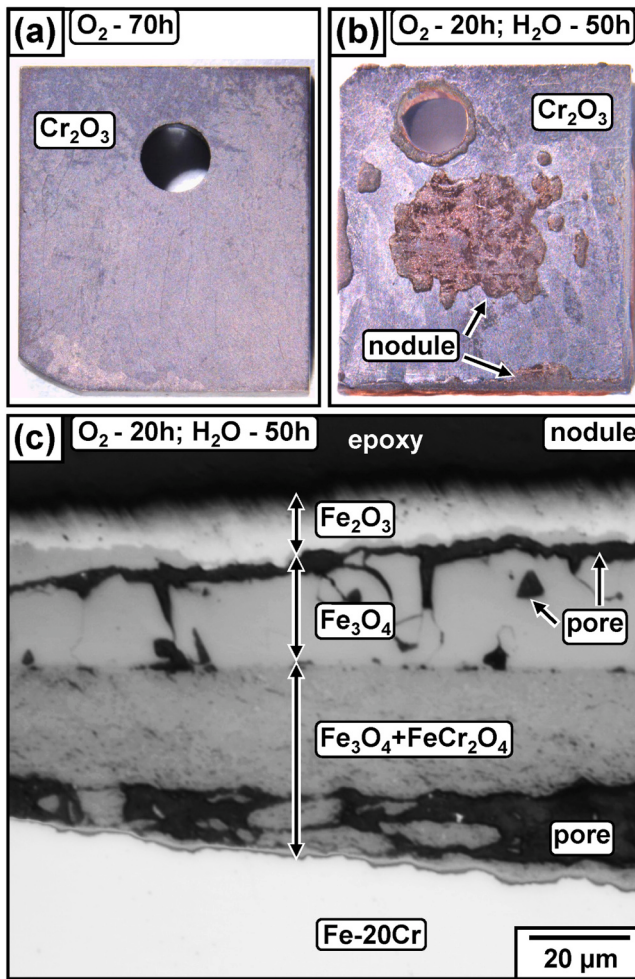


**Fig. 8.** Optical microscope images: surface views of Fe-20Cr (a) oxidised in Ar-20 O<sub>2</sub> (750 °C, 70 h) and (b) after a two-stage reaction (Ar-20 O<sub>2</sub> for 20 h and then Ar-20 H<sub>2</sub>O for 50 h, 750 °C), and (c) cross-section of nodules in (b).

Although deionised water (H<sub>2</sub><sup>16</sup>O) and pure oxygen (<sup>16</sup>O<sub>2</sub>) had been used to form reaction gases, two oxygen isotopes <sup>18</sup>O<sup>-</sup> and <sup>16</sup>O<sup>-</sup> were detected in the Cr<sub>2</sub>O<sub>3</sub> scales formed in all gases (Figs. 20, 21, 22). The intensity of <sup>18</sup>O<sup>-</sup> was weaker than that of <sup>16</sup>O<sup>-</sup> in all cases.

#### 4. Discussion

The relative alloy oxidation rates produced in different gases (Fig. 1) are clearly correlated with the changed nature of the reaction products (Tables 2 and 3). At 750 °C, the Fe-20Cr alloy formed a uniform, slow-growing Cr<sub>2</sub>O<sub>3</sub> scale in Ar-20O<sub>2</sub>, but failed to do so in water vapour gases at this temperature. Fast growing Fe-rich oxide nodules developed in Ar-20H<sub>2</sub>O, leading to much faster weight uptake rates. Similar nodules also developed in Ar-20H<sub>2</sub>O-5H<sub>2</sub>, but over a smaller surface area fraction, leading to an intermediate rate of weight increase.

At 850 °C, formation of a uniform Cr<sub>2</sub>O<sub>3</sub> scale was more favoured: protective scales grow at similar rates in both Ar-20O<sub>2</sub> and Ar-5H<sub>2</sub>O. The addition of H<sub>2</sub> to water vapour slightly accelerated chromia scale growth, and further increased weight uptake by growing an additional spinel layer on parts of the chromia surface.

Attention is focused here on the underlying causes of these different effects, including in particular changes to the nature of the chromia layer itself. Effects of the reaction temperature and hydrogen on oxidation in water vapour are now considered in terms of thermodynamics and kinetics.

#### 4.1. Failure of Cr<sub>2</sub>O<sub>3</sub> scales in Ar-20H<sub>2</sub>O-(5H<sub>2</sub>) at 750 °C

##### 4.1.1. Local, fast Cr<sub>2</sub>O<sub>3</sub> scale growth in Ar-20H<sub>2</sub>O

The Fe-20Cr alloy formed chromia scales in Ar-20O<sub>2</sub> and Ar-20 H<sub>2</sub>O at 750 °C (Fig. 10). However, Fe-rich oxide nodules developed quickly in Ar-20H<sub>2</sub>O (Figs. 2, 3), resulting in high weight uptakes (Fig. 1a).

For protection, the alloy must have sufficient Cr supply via alloy diffusion to the scale-alloy interface to maintain exclusive chromia scale growth. This criterion leads to the critical alloy Cr concentration [16]:

$$N_{\text{Cr}}^{\text{crit}} = \frac{V_m}{V_{\text{CrO}_{1.5}}} \left( \frac{\pi k_p}{2 \tilde{D}_{\text{Cr}}} \right)^{\frac{1}{2}} \quad (1)$$

Here  $V_m = 7.3 \text{ cm}^3/\text{mol}$  and  $V_{\text{CrO}_{1.5}} = 14.6 \text{ cm}^3/\text{mol}$  are the molar volumes of alloy and oxide and  $\tilde{D}_{\text{Cr}}$  is the alloy interdiffusion coefficient of Cr. If the scale is pure Cr<sub>2</sub>O<sub>3</sub>,  $k_p$  is the parabolic rate constant for scale thickening

$$X^2 = 2k_p t \quad (2)$$

with  $X$  the scale thickness and  $t$  time.

The value  $k_p = 7.1 \times 10^{-15} \text{ cm}^2/\text{s}$  for Fe-20Cr oxidised in Ar-20O<sub>2</sub> was estimated from (2) using the chromia scale's average thickness after 70 h reactions at 750 °C (Table 2). In the case of reaction in Ar-20H<sub>2</sub>O, growth of Cr<sub>2</sub>O<sub>3</sub> scales was significantly non-uniform at the initial stage, resulting in local, thicker Cr<sub>2</sub>O<sub>3</sub> scales (Fig. 4a). For this reason, thickness of the Cr<sub>2</sub>O<sub>3</sub> scale (150 nm) near a fine Fe-rich oxide nodule after reaction for 20 min (Fig. 4b) and that after reaction for 70 h (Fig. 10d, Table 2) were used, yielding  $k_p = 9.4 \times 10^{-14}$  (20 min) and  $7.9 \times 10^{-16} \text{ cm}^2/\text{s}$  (70 h). The  $\tilde{D}_{\text{Cr}} = 6.4 \times 10^{-13} \text{ cm}^2/\text{s}$  value of Fe-20Cr was taken as volume diffusion coefficient from [17] for ferritic Fe-12Cr-Mo-V steel. The calculated  $N_{\text{Cr}}^{\text{crit}}$  values are 0.07 in Ar-20O<sub>2</sub>, 0.24 in Ar-20H<sub>2</sub>O with  $k_p$ (20 min), and 0.02 in Ar-20H<sub>2</sub>O with  $k_p$ (70 h), indicating correctly that Fe-20Cr (alloy Cr concentration  $N_{\text{Cr}} = 0.21$ ) is able to maintain a Cr<sub>2</sub>O<sub>3</sub> scale in Ar-20O<sub>2</sub>.

For the reaction in Ar-20H<sub>2</sub>O, the theory correctly predicts that Fe-20Cr ( $N_{\text{Cr}} = 0.21$ ) fails to maintain the Cr<sub>2</sub>O<sub>3</sub> scale based on the  $k_p$  estimated after 20 min, but can maintain the scale if it grows at the slower  $k_p$  estimated after 70 h. The experimental results (Table 2) are consistent with the prediction. The Cr<sub>2</sub>O<sub>3</sub> scale lasted longer in Ar-20O<sub>2</sub>, but local surface regions on Fe-20Cr covered by fast growing Cr<sub>2</sub>O<sub>3</sub> scales at the initial stage in Ar-20H<sub>2</sub>O underwent breakaway oxidation. Scale growth was faster in H<sub>2</sub>O, and consequent alloy depletion in Cr led to failure. However, on other parts of the alloy surface, the protective scale survived. It is clear the alloy is marginal in this gas, and it is noted that calculated critical  $N_{\text{Cr}}$  values are dependent on input factors, including local variations in  $k_p$ .

The measured surface areas of nodules after reactions for 20 min and 70 h in Ar-20H<sub>2</sub>O were about 2 and 36 %, respectively. It is concluded that the alloy Cr concentration of Fe-20Cr was not sufficient to maintain fast growing Cr<sub>2</sub>O<sub>3</sub> scales on local surface regions during the reaction, resulting in local breakaway of the Cr<sub>2</sub>O<sub>3</sub> scale and formation of new Fe-rich oxide nodules.

The Cr<sub>2</sub>O<sub>3</sub> scale grown in the two-stage reaction was made up of fine and coarse grains (Fig. 9d), whilst that formed in Ar-20 O<sub>2</sub> for 70 h contained coarser grains (Fig. 9b, Table 2). Whereas chromia scales grown in O<sub>2</sub> alone are stable, those produced in the two-stage experiment suffer local breakaway. It is clear that properties of the Cr<sub>2</sub>O<sub>3</sub> scale preformed in Ar-20O<sub>2</sub> must have changed when exposed to Ar-20 H<sub>2</sub>O, allowing locally accelerated Cr<sub>2</sub>O<sub>3</sub> scale growth, causing local Cr depletion in the underlying alloy and consequently breakaway.

Examination of TEM images of the Cr<sub>2</sub>O<sub>3</sub> scales grown in O<sub>2</sub> (20 h), H<sub>2</sub>O (70 h), and O<sub>2</sub> (20 h) then H<sub>2</sub>O (50 h) (Fig. 10a, d, e) reveals no obvious difference in oxide grain size or columnar morphology. Thus the average grain boundary density does not account for the different behaviour. Instead, the properties of some, but not all, grain boundaries

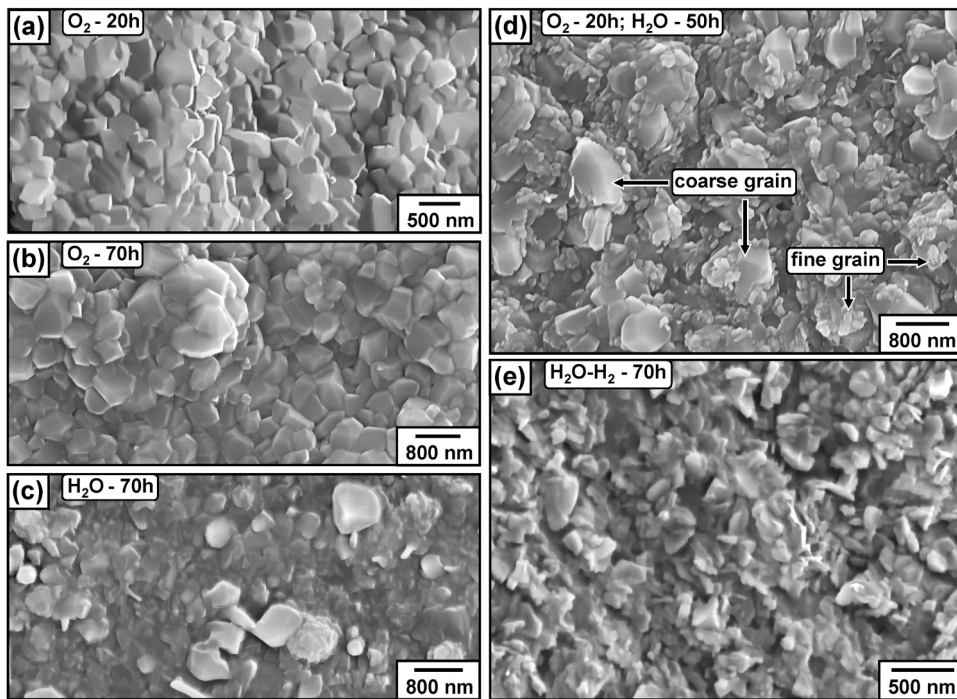
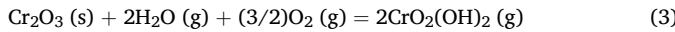


**Fig. 9.** SE-SEM top views of  $\text{Cr}_2\text{O}_3$  scales formed on Fe-20Cr at 750 °C in: (a) Ar-20 $\text{O}_2$  (20 h), (b) Ar-20 $\text{O}_2$  (70 h), (c) Ar-20 $\text{H}_2\text{O}$  (70 h), (d) 2-stages (Ar-20 $\text{O}_2$  for 20 h and then Ar-20 $\text{H}_2\text{O}$  for 50 h), and (e) Ar-20 $\text{H}_2\text{O}$ -5 $\text{H}_2$  (70 h).

have changed, allowing faster diffusion of both Cr and Fe. The simplest hypothesis is that  $\text{H}_2\text{O}$  (g)-derived species had entered some chromia grain boundaries in  $\text{H}_2\text{O}$ -containing gases.

Failure of  $\text{Cr}_2\text{O}_3$  scales in water vapour at high temperatures can in principle be caused by the volatilisation reaction, resulting in Cr depletion in the underlying alloy and breakaway of the  $\text{Cr}_2\text{O}_3$  scale [18]



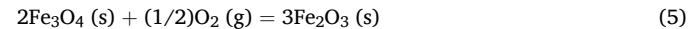
In this study, however, the oxygen partial pressure of Ar-20 $\text{H}_2\text{O}$  was small (Table 1), and volatilisation of  $\text{Cr}_2\text{O}_3$  is therefore negligible.

#### 4.1.2. Failure of $\text{Cr}_2\text{O}_3$ scale in Ar-20 $\text{H}_2\text{O}$ -5 $\text{H}_2$

The Fe-20Cr alloy oxidised in Ar-20 $\text{H}_2\text{O}$  and Ar-20  $\text{H}_2\text{O}$ -5 $\text{H}_2$  at 750 °C formed iron rich oxide nodules and  $\text{Cr}_2\text{O}_3$  scales (Table 1). The chromia scale growth rate  $k_p = 2.4 \times 10^{-15} \text{ cm}^2/\text{s}$  for Fe-20Cr oxidised in Ar-20 $\text{H}_2\text{O}$ -5 $\text{H}_2$  was estimated from (2) using the chromia scale's average thickness after 70 h reaction at 750 °C (Table 2). The  $N_{\text{Cr}}^{\text{crit}} = 0.04$  value calculated from (1) in Ar-20 $\text{H}_2\text{O}$ -5 $\text{H}_2$  indicates that the alloy Cr concentration is able to maintain the chromia scale growth, in disagreement with the experimental results. The difference may be caused by variable  $\text{Cr}_2\text{O}_3$  scale thickness on local sample surface regions, as in the case of oxidation in Ar-20  $\text{H}_2\text{O}$  discussed above.

The  $\text{Cr}_2\text{O}_3$  scale formed in Ar-20 $\text{H}_2\text{O}$ -5 $\text{H}_2$  consisted of an outer, fine-grained layer and an inner, coarse-grained layer (Fig. 10f), whilst only a single scale layer formed in Ar-20 $\text{H}_2\text{O}$  (Fig. 10d). The addition of  $\text{H}_2$  to Ar-20  $\text{H}_2\text{O}$  significantly reduced  $p_{\text{O}_2}$  but increased  $p_{\text{H}_2}$  in the reaction gas. The changed chromia microstructure reflects different outcomes of the competition between grain nucleation and growth, both processes being susceptible to modification by hydrogen. The balance between them may change with scale thickness as a result of slowing diffusion, but details are not revealed by present results. The key question, however, is what effect  $\text{H}_2$  had on the onset of breakaway: the nucleation and growth of Fe-rich oxide nodules.

Formation of  $\text{Fe}_2\text{O}_3$  and  $\text{Fe}_3\text{O}_4$  is controlled by reactions:



The equilibrium oxygen partial pressures ( $p_{\text{O}_2}$ ) of (4) and (5) at 750 °C calculated using activity of Fe in the alloy ( $a_{\text{Fe}} = 0.79$ , the maximum possible at a chromia scale surface) are  $1.9 \times 10^{-20}$  and  $1.7 \times 10^{-11}$  atm, respectively. It is clear that  $p_{\text{O}_2}$  values of Ar-20 $\text{H}_2\text{O}$  ( $6.5 \times 10^{-8}$  atm) and Ar-20 $\text{H}_2\text{O}$ -5 $\text{H}_2$  ( $4.6 \times 10^{-19}$  atm) at 750 °C are sufficient to stabilise  $\text{Fe}_3\text{O}_4$ , whilst  $\text{Fe}_2\text{O}_3$  is stable only in Ar-20 $\text{H}_2\text{O}$ , consistent with the experimental results (Fig. 5). The  $\text{Fe}_3\text{O}_4$  scale layer grew faster in Ar-20  $\text{H}_2\text{O}$  (Table 2) than in Ar-20 $\text{H}_2\text{O}$ -5 $\text{H}_2$  (Table 2) because  $p_{\text{O}_2} = 1.7 \times 10^{-11}$  atm set by reaction (5) was higher than that in Ar-20 $\text{H}_2\text{O}$ -5 $\text{H}_2$  ( $4.6 \times 10^{-19}$  atm). As a result, Fe-rich oxide nodules spread faster in Ar-20  $\text{H}_2\text{O}$  (Table 2), resulting in higher weight gains at 750 °C (Fig. 1a).

#### 4.1.3. Effects of oxygen partial pressures and grain sizes on $\text{Cr}_2\text{O}_3$ scale growth

Addition of  $\text{H}_2$  to Ar-20  $\text{H}_2\text{O}$  reduced oxygen partial pressure (Table 1) and  $\text{Cr}_2\text{O}_3$  grain sizes (Table 2). Parabolic rate constants for  $\text{Cr}_2\text{O}_3$  scale growth calculated from (2) for 70 h reactions are  $7.9 \times 10^{-16}$  (Ar-20 $\text{H}_2\text{O}$ ) and  $2.4 \times 10^{-15} \text{ cm}^2/\text{s}$  (Ar-20 $\text{H}_2\text{O}$ -5 $\text{H}_2$ ). The ratio between  $k_p$  values is

$$\frac{k_p^{\text{H}_2\text{O}}}{k_p^{\text{H}_2\text{O}-\text{H}_2}} = \frac{7.9 \times 10^{-16}}{2.4 \times 10^{-15}} = 0.3 \quad (6)$$

The inert  $\text{SiO}_2$  marker results (Figs. 18, 19) indicated that the  $\text{Cr}_2\text{O}_3$  scale grew mainly by outward diffusion of Cr in Ar-20 $\text{H}_2\text{O}$ -(5 $\text{H}_2$ ). Assuming that mobile species are ionic and at local equilibrium with surrounding oxide, the parabolic rate constant can be evaluated from Wagner's scaling theory [19,20] for *p*- and *n*-type  $\text{Cr}_2\text{O}_3$ , now considered separately.

Formation reactions for point defects can be written as

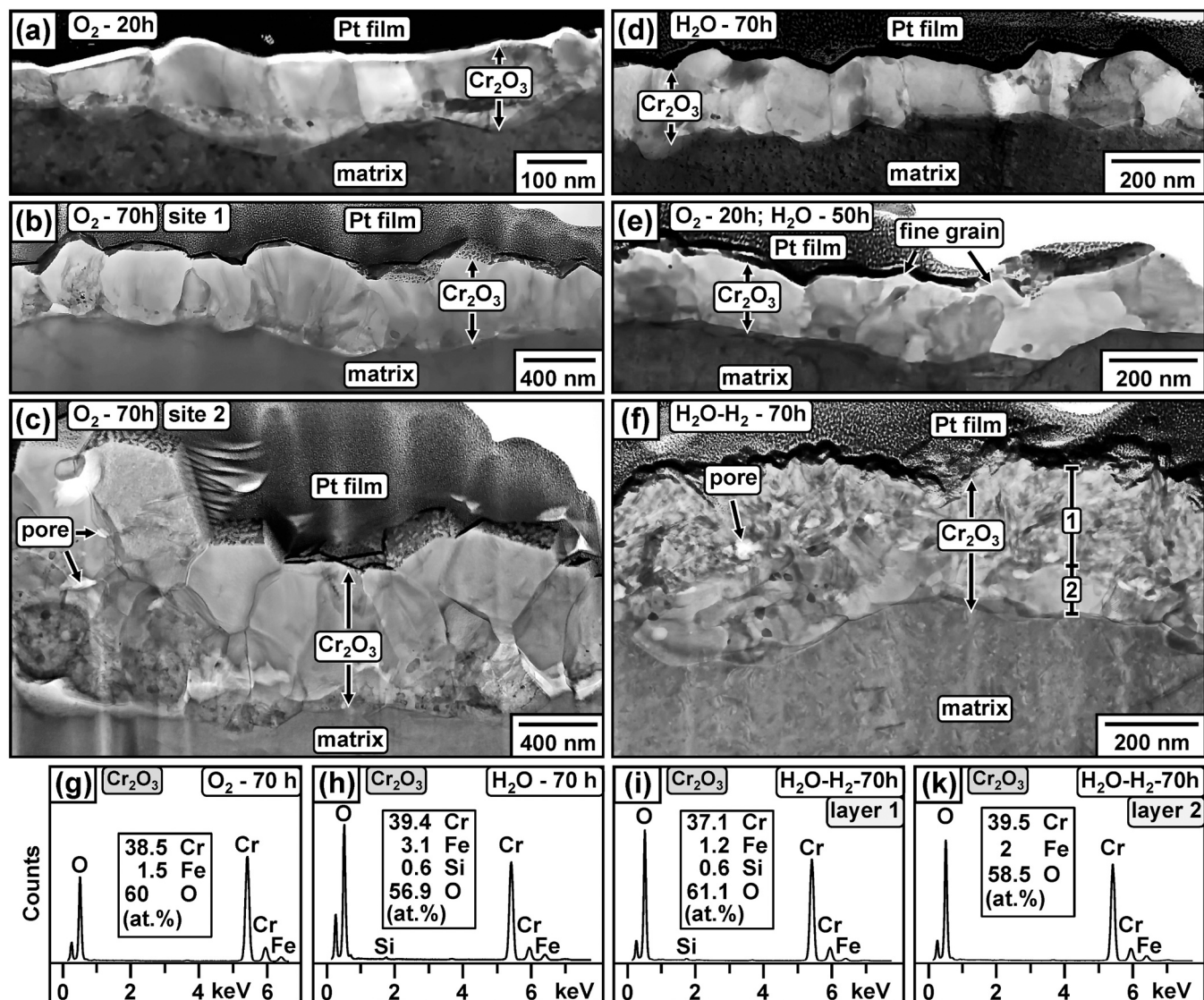


**Fig. 10.** BF-STEM cross-sections of Cr<sub>2</sub>O<sub>3</sub> scales formed on Fe-20Cr at 750 °C in: (a) Ar-20O<sub>2</sub> (20h), (b, c) Ar-20O<sub>2</sub> (70 h), (d) Ar-20H<sub>2</sub>O (70 h), (e) 2-stages (Ar-20O<sub>2</sub> for 20 h and then Ar-20H<sub>2</sub>O for 50 h), (f) Ar-20H<sub>2</sub>O-5H<sub>2</sub> (70 h), and EDX spectra of Cr<sub>2</sub>O<sub>3</sub> scales formed in (g) O<sub>2</sub>-70 h, (h) H<sub>2</sub>O-70 h, and (i, k) H<sub>2</sub>O-H<sub>2</sub>-70 h for layers 1 and 2 in (f).

**Table 2**  
Thin scales and nodules at 750 °C.

Gas	Thin scale			Nodules	
	Phase	X (nm)	Grains (nm) <sup>*</sup>	Oxide Layers (μm)	Area coverage (%)
Ar-20 O <sub>2</sub> (20 h)	Cr <sub>2</sub> O <sub>3</sub>	120±50	130±60 (C)	-	-
Ar-20 O <sub>2</sub> (70 h)	Cr <sub>2</sub> O <sub>3</sub>	600±300	400±200 (C)	-	-
Ar-20 H <sub>2</sub> O (20 min)	Cr <sub>2</sub> O <sub>3</sub>	max 150±30	-	Fe <sub>2</sub> O <sub>3</sub> : 0.8±0.2 (Cr,Fe)O <sub>x</sub> : 0.4±0.2 Cr <sub>2</sub> O <sub>3</sub> : 0.2±0.1	2
Ar-20 H <sub>2</sub> O (70 h)	Cr <sub>2</sub> O <sub>3</sub>	200±20	130±20 (C)	Fe <sub>2</sub> O <sub>3</sub> : 13±5 Fe <sub>3</sub> O <sub>4</sub> : 45±5 Fe <sub>3</sub> O <sub>4</sub> +FeCr <sub>2</sub> O <sub>4</sub> : 50±6	36
Two stages (O <sub>2</sub> -20 h, H <sub>2</sub> O-50 h)	Cr <sub>2</sub> O <sub>3</sub>	250±80	40–175 (C)	Fe <sub>2</sub> O <sub>3</sub> : 8±3 Fe <sub>3</sub> O <sub>4</sub> : 20±2 Fe <sub>3</sub> O <sub>4</sub> +FeCr <sub>2</sub> O <sub>4</sub> : 24±2	14
Ar-20 H <sub>2</sub> O-5 H <sub>2</sub> (70 h)	Cr <sub>2</sub> O <sub>3</sub>	350±100	-Outer layer: 18±4 (E) -Inner layer: 120±60 (E)	Fe <sub>3</sub> O <sub>4</sub> : 30±10 Fe <sub>3</sub> O <sub>4</sub> +FeCr <sub>2</sub> O <sub>4</sub> : 31±6	14

\* C: columnar, E: equiaxed, X: thickness.

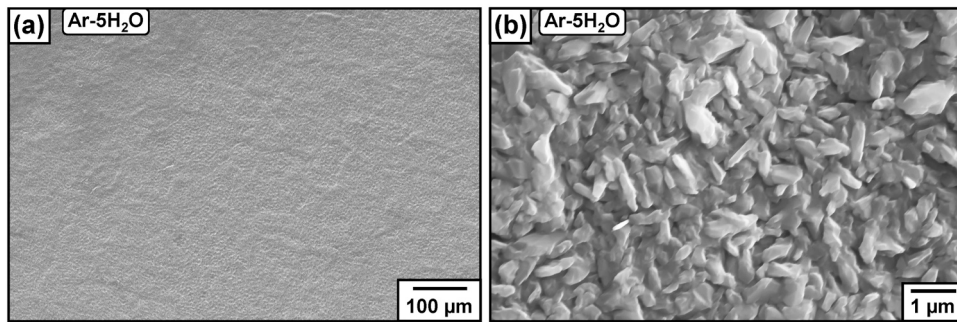


Fig. 11. Fe-20Cr oxidized for 70 h at 850 °C in Ar-5H<sub>2</sub>O: (a) SE-SEM top view and (b) high magnification image.

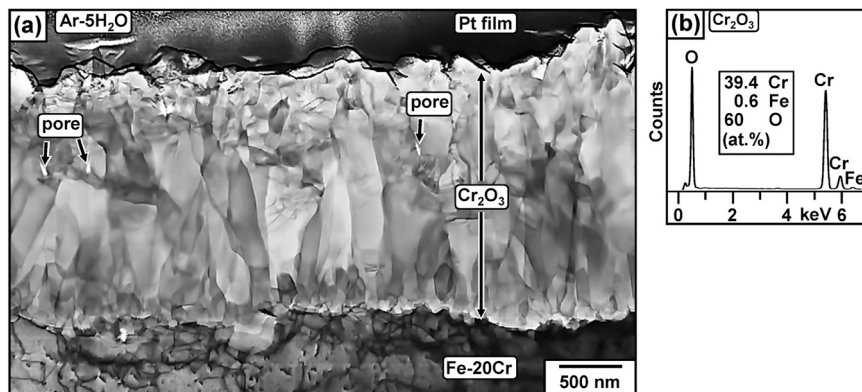


Fig. 12. Fe-20Cr reacted at 850 °C for 70 h in Ar-5H<sub>2</sub>O: (a) BF-STEM cross-section and (b) EDX spectrum of Cr<sub>2</sub>O<sub>3</sub> scale.

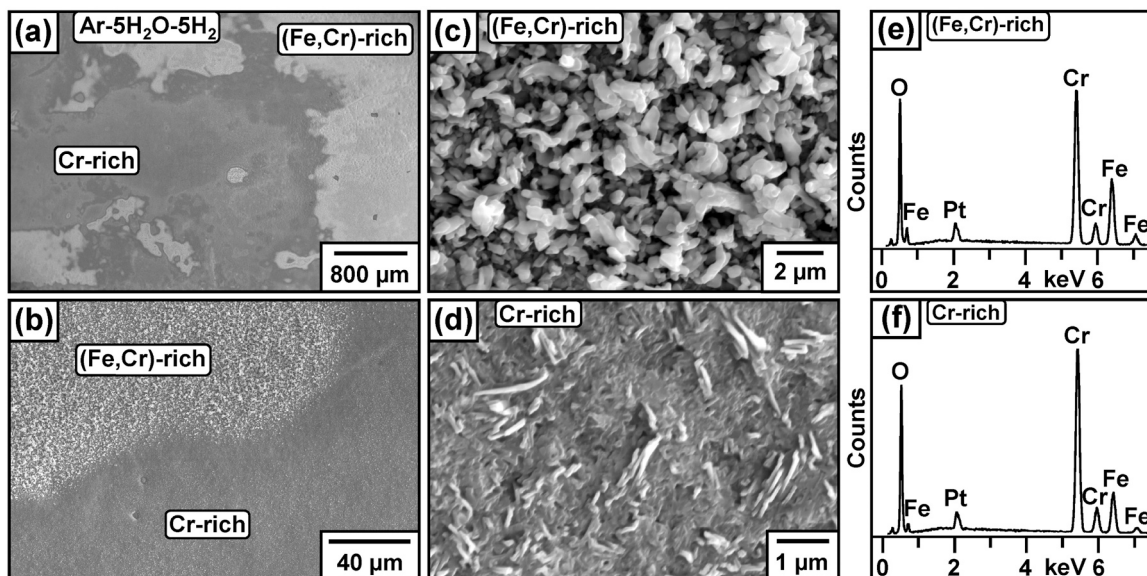
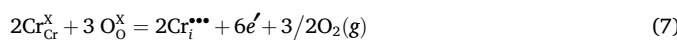


Fig. 13. Fe-20Cr oxidized for 70 h at 850 °C in Ar-5 H<sub>2</sub>O-5 H<sub>2</sub>: (a) SE-SEM top view, (b) high magnification image of (a), high magnification images and EDX spectra of (c, e) (Fe-Cr)-rich and (d, f) Cr-rich areas in (b). Pt coating was deposited prior to SEM analysis.



#### p-type chromia

The parabolic rate constant can be approximated from Wagner's scaling theory [19,20]

$$k_p = \text{const.} D_{\text{Cr}}^{\text{eff}} p_{\text{O}_2}^{3/16} \quad (9)$$

with  $D_{\text{Cr}}^{\text{eff}}$  the effective diffusion coefficient of Cr in the scale and  $p_{\text{O}_2}$  equilibrium partial pressure of oxygen in reaction gases (Table 1). The  $D_{\text{Cr}}^{\text{eff}}$  value results from contributions by grain boundary diffusion ( $D_{\text{Cr}}^{\text{gb}}$ ) and lattice diffusion ( $D_{\text{Cr}}^{\ell}$ )

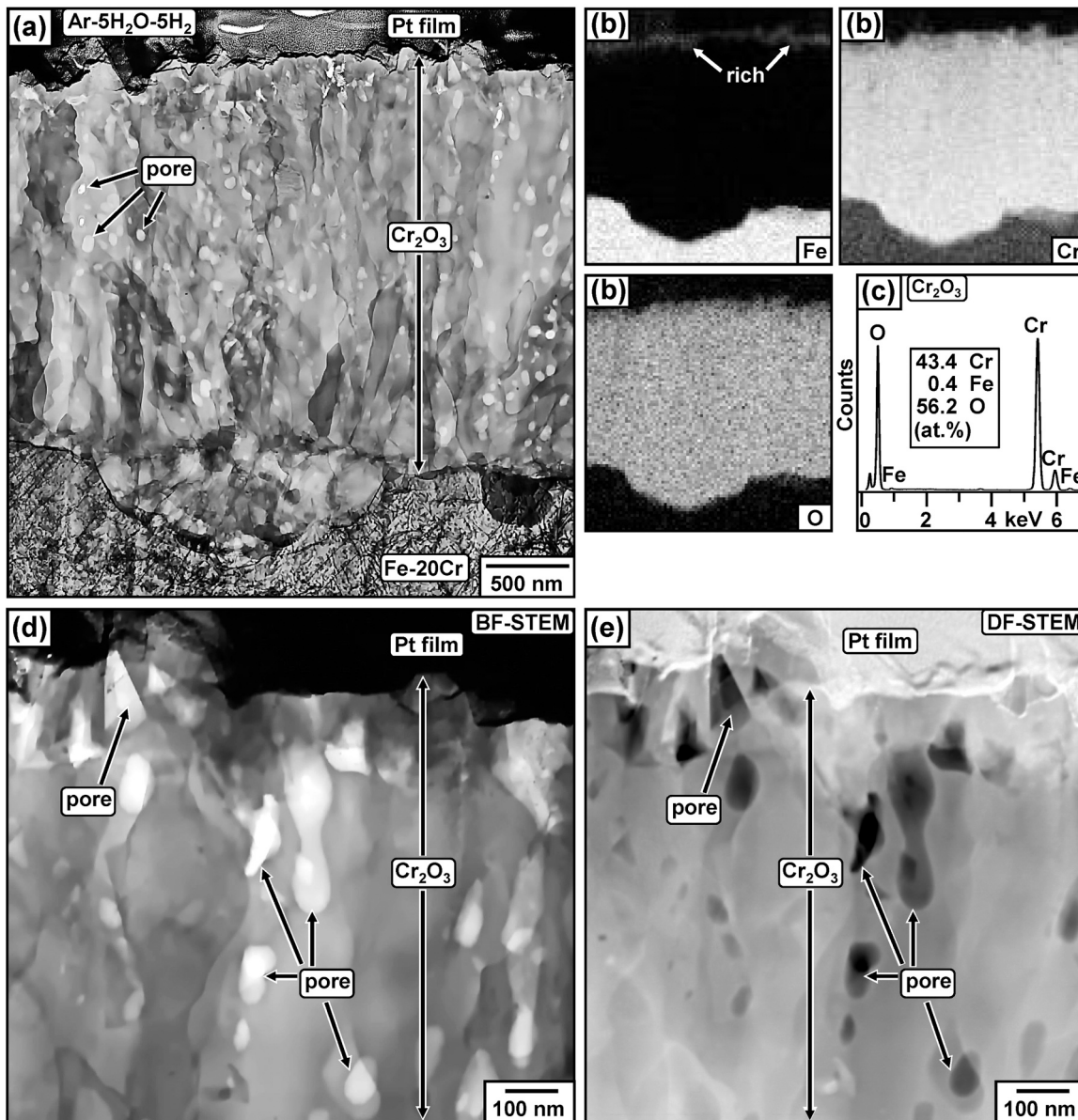


**Fig. 14.** Fe-20Cr reacted at 850 °C for 70 h in Ar-5 H<sub>2</sub>O-5 H<sub>2</sub>: (a) BF-STEM cross-section of Cr-rich area in Fig. 13b, (b) EDX mapping, (c) EDX spectrum of Cr<sub>2</sub>O<sub>3</sub> scale in (a), and (d) BF-STEM and (e) DF-STEM high magnification images of (a), showing pores in bright and dark contrasts.

$$D_{\text{Cr}}^{\text{eff}} = f D_{\text{Cr}}^{\text{gb}} + (1-f) D_{\text{Cr}}^{\ell} \quad (10)$$

$$f = \frac{q\delta}{d} \quad (11)$$

with  $q$  a factor based on grain shape,  $\delta$  grain boundary width, and  $d$  average grain size. The cross-sections of grains formed in Ar-20 H<sub>2</sub>O (5 H<sub>2</sub>) at 750 °C are approximated as square (Fig. 10d, f). Since  $D_{\text{Cr}}^{\text{gb}} >> D_{\text{Cr}}^{\ell}$  [21,22], the  $D_{\text{Cr}}^{\text{eff}}$  value is approximated by

$$D_{\text{Cr}}^{\text{eff}} = \frac{q\delta}{d} D_{\text{Cr}}^{\text{gb}} \quad (12)$$

The average oxide grain size  $d$  is 130 nm in Ar-20 H<sub>2</sub>O (Table 2). The Cr<sub>2</sub>O<sub>3</sub> scale grown in Ar-20 H<sub>2</sub>O-5 H<sub>2</sub> consisted of fine- and coarse-grained layers (Table 2), with an average grain size of 69 nm. Substitution of (12) and values of  $d$  and  $p_{\text{O}_2}$  (Table 1) into (9) leads to a predicted rate ratio

$$\frac{k_p^{\text{H}_2\text{O}}}{k_p^{\text{H}_2\text{O}-\text{H}_2}} = \frac{d(\text{H}_2\text{O} - \text{H}_2)}{d(\text{H}_2\text{O})} \times \frac{p_{\text{O}_2}^{3/16}(\text{H}_2\text{O})}{p_{\text{O}_2}^{3/16}(\text{H}_2\text{O} - \text{H}_2)} \quad (13)$$

and at 750 °C

$$\frac{k_p^{\text{H}_2\text{O}}}{k_p^{\text{H}_2\text{O}-\text{H}_2}} = 65 \quad (14)$$

Rate ratios are summarized in Table 4. It is clear that the calculated ratio of 65 differs strongly from the experimental ratio of 0.3, indicating that the assumption of *p*-type behaviour is incorrect.

#### n-type chromia

$$k_p = \text{const.} \cdot D_{\text{Cr}}^{\text{eff}} \cdot \left( p_{\text{O}_2}^{\text{equ}} \right)^{-3/16} \quad (15)$$

with  $p_{\text{O}_2}^{\text{equ}}$  partial pressure of oxygen set by equilibrium Cr/Cr<sub>2</sub>O<sub>3</sub> at the

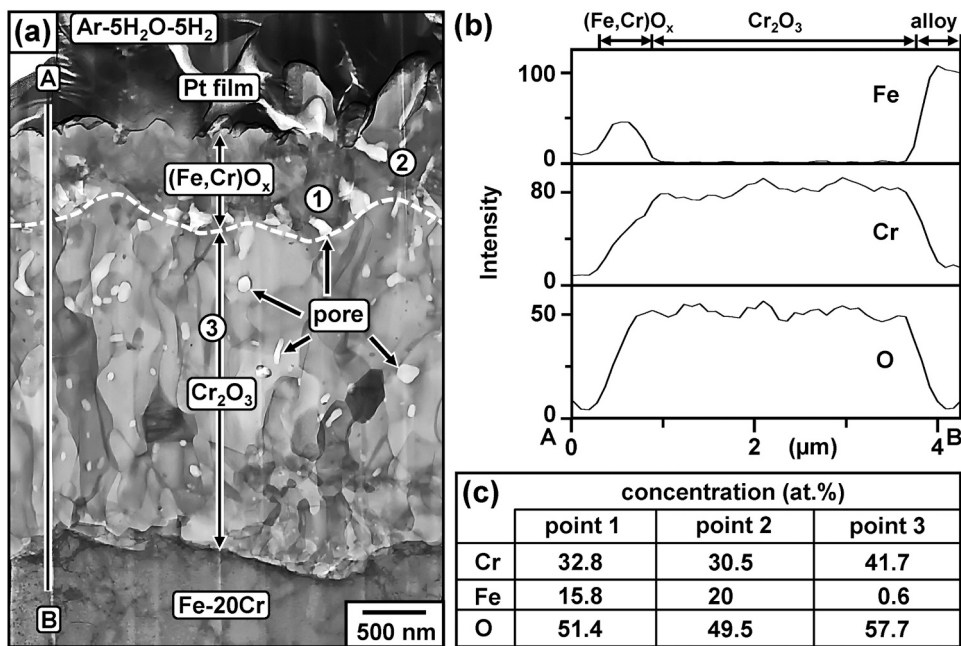


**Fig. 15.** Fe-20Cr reacted at 850 °C for 70 h in Ar-5 H<sub>2</sub>O-5 H<sub>2</sub>: (a) BF-STEM cross-section of Fe-rich area in Fig. 13b, (b) EDX line profiles along A-B in (a), and (c) EDX concentrations of points 1-3 in (a).

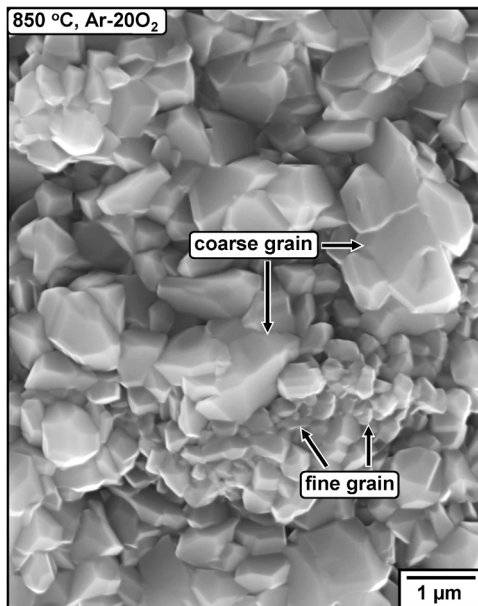


**Fig. 16.** SE-SEM surface view of Fe-20Cr reacted at 850 °C for 70 h in Ar-20O<sub>2</sub>.

scale-alloy interface.



$$\left(p_{\text{O}_2}^{\text{equ}}\right)^{3/2} = \frac{a_{\text{Cr}_2\text{O}_3}}{K_{14}a_{\text{Cr}}^2} \quad (17)$$

with  $K_{14}$  equilibrium constant for (16) and  $a_{\text{Cr}_2\text{O}_3} = 1$  activity of Cr<sub>2</sub>O<sub>3</sub>. Activity of Cr at the scale-alloy interface,  $a_{\text{Cr}}$ , is controlled by mol fraction of Cr in the alloy beneath the scale ( $N_{\text{Cr}}$ ) and activity coefficient ( $\gamma$ )

$$a_{\text{Cr}} = \gamma \times N_{\text{Cr}} \quad (18)$$

The thickness difference of Cr<sub>2</sub>O<sub>3</sub> scales formed in Ar-20 H<sub>2</sub>O (200 ± 20 nm thick) and Ar-20H<sub>2</sub>O-5H<sub>2</sub> (350 ± 100 nm thick) is not great. On this basis, the Cr depletion in the underlying alloys is expected to be nearly the same for both gases, and consequently the  $p_{\text{O}_2}^{\text{equ}}$  ratio for the two gases is approximated as 1.

The rate ratio is

$$\frac{k_p^{\text{H}_2\text{O}}}{k_p^{\text{H}_2\text{O}-\text{H}_2}} = \frac{d(\text{H}_2\text{O} - \text{H}_2)}{d(\text{H}_2\text{O})} \quad (19)$$

and at 750 °C

$$\frac{k_p^{\text{H}_2\text{O}}}{k_p^{\text{H}_2\text{O}-\text{H}_2}} = 0.5 \quad (20)$$

This value is much closer to that calculated from experimental scale thicknesses to be 0.3. On this basis, it is concluded that the Cr<sub>2</sub>O<sub>3</sub> scales developed at 750 °C in Ar-20H<sub>2</sub>O-(5H<sub>2</sub>) were not *p*-type, in agreement with previous reports [23,24] on chromia semiconductor properties. The reduction in  $p_{\text{O}_2}$  by addition of H<sub>2</sub> to Ar-20H<sub>2</sub>O (Table 1) had an effect on scale boundary conditions which was unimportant. However, the smaller Cr<sub>2</sub>O<sub>3</sub> grains formed in Ar-20H<sub>2</sub>O-5H<sub>2</sub> increase the number of intergranular diffusion pathways, resulting in thicker scales.

#### 4.2. Scale growth mechanism in H<sub>2</sub>O-(H<sub>2</sub>)

In this work, SiO<sub>2</sub> powder was chosen to mark the original sample surface because no interdiffusion occurs between SiO<sub>2</sub> and the underlying alloy, and solubility of SiO<sub>2</sub> in Cr<sub>2</sub>O<sub>3</sub> is negligible [25]. In addition, fine silica grains (< 0.2 μm) /clusters scattered over the sample surface provided minimum obstruction to transport of both metal and oxidising species during reactions. The experimental results in Ar-5 H<sub>2</sub>O (Fig. 18) and Ar-5H<sub>2</sub>O-5H<sub>2</sub> (Fig. 19) revealed the SiO<sub>2</sub> marker close to the Cr<sub>2</sub>O<sub>3</sub> scale-alloy interface. Therefore, it is concluded that the Cr<sub>2</sub>O<sub>3</sub> scales

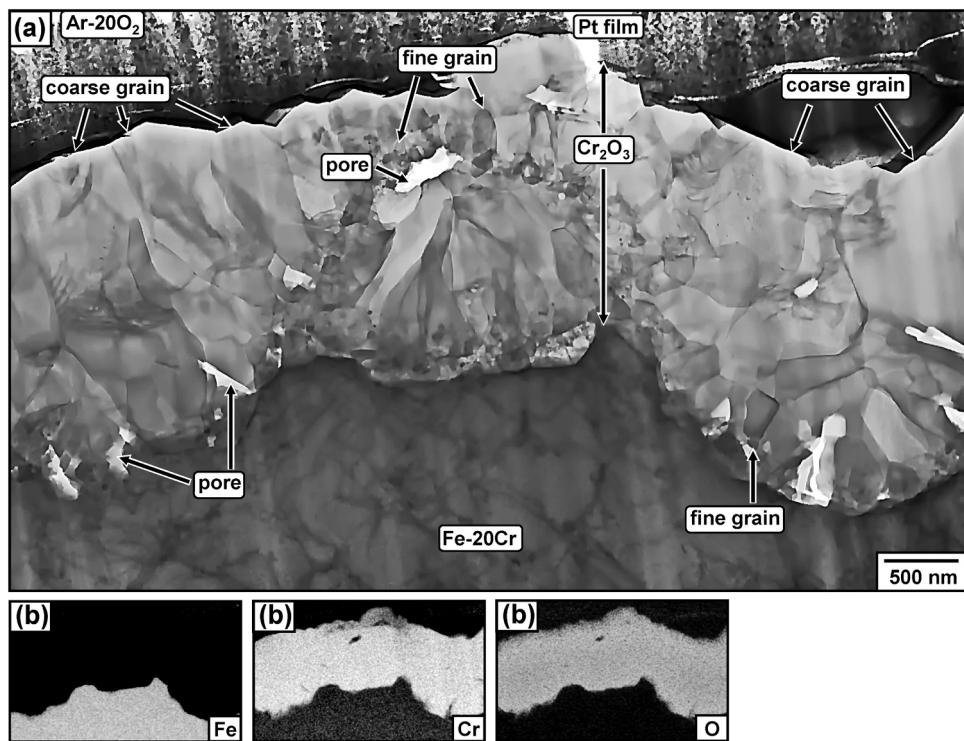


**Fig. 17.** Fe-20Cr reacted at 850 °C for 70 h in Ar-20O<sub>2</sub>: (a) BF-STEM cross-section and (b) EDX mapping.

**Table 3**

Thin scales at 850 °C.

Gas	Thin scale		
	Phase	X (nm)	Grains (nm)*
Ar-20 O <sub>2</sub> (70 h)	Cr <sub>2</sub> O <sub>3</sub>	1900±500	45–1270 (E)
Ar-5 H <sub>2</sub> O (70 h)	Cr <sub>2</sub> O <sub>3</sub>	1800±200	– Columnar grain: 150±100 (W), max 1120 (L) – Equiaxed grain: max 240
Ar-5 H <sub>2</sub> O-5 H <sub>2</sub> (70 h)	Cr <sub>2</sub> O <sub>3</sub>	2600±200	– Columnar grain: 130±40 (W), max 1140 (L) – Equiaxed grain: max 450

\* W: width, L: length, E: equiaxed, X: thickness.

grew mainly by outward Cr diffusion in Ar-5H<sub>2</sub>O-(5H<sub>2</sub>) at 850 °C. Assuming temperature has little effect on relative mass transport contributions, this marker result was consistent with the observation of fine Cr<sub>2</sub>O<sub>3</sub> grains formed in Ar-20H<sub>2</sub>O on top of coarser Cr<sub>2</sub>O<sub>3</sub> grains performed in Ar-20 O<sub>2</sub> in the two-stage experiment at 750 °C (Fig. 9d).

Chromia grains formed in Ar-5H<sub>2</sub>O-(5H<sub>2</sub>) at 850 °C were fine and equiaxed after reactions for 24 h (Figs. 18, 19). When the reactions continued to 70 h, these grains joined and grew to coarser, columnar grains (Figs. 12, 14, 15). Some columnar grains started to form randomly near the scale-alloy interface after the reaction for 24 h in Ar-5 H<sub>2</sub>O (Fig. 18).

Chromia scale growth mechanism in water vapour has been studied by depth profiling of a Cr<sub>2</sub>O<sub>3</sub> scale developed on Fe-15Cr-0.5Si in Ar-15 H<sub>2</sub><sup>16</sup>O/Ar-15 H<sub>2</sub><sup>18</sup>O at 800 °C [26], showing the Cr<sub>2</sub>O<sub>3</sub> scale grows by inward transport of oxygen bearing species. This result is not consistent with the current SiO<sub>2</sub> marker result. The isotope marker method relies on location of <sup>18</sup>O peaks in SIMS depth profiling analysis of a Cr<sub>2</sub>O<sub>3</sub> scale grown in a two-stage oxidation (first in H<sub>2</sub><sup>16</sup>O and then in H<sub>2</sub><sup>18</sup>O). The SiO<sub>2</sub> marker result in this study is visible using TEM/EDX mapping to detect SiO<sub>2</sub> in a Cr<sub>2</sub>O<sub>3</sub> scale, clearly showing its locations (Figs. 18, 19). The difference between the two results reflects the complexity of comparing Cr<sub>2</sub>O<sub>3</sub> scale growth on different alloys.

Whilst the marker experiment design succeeded in avoiding the blockage of mass transfer, it nonetheless affected chromia grain nucleation, leading to finer grained scales in regions where SiO<sub>2</sub> particles were located (Figs. 18, 19). Since the marker silica grains were sprayed onto the sample surface before reactions, narrow gaps may form between SiO<sub>2</sub> grains and the sample surface. These gaps provided a short diffusion path for reaction gas to bypass silica grains and then oxidise the underlying alloy surface at the initial reaction stage. For this reason, a thin, intermediate Cr<sub>2</sub>O<sub>3</sub> layer may form between the silica grains/clusters and sample surface (Figs. 18, 19).

#### 4.3. Oxidation in Ar-5H<sub>2</sub>O-(5H<sub>2</sub>) at 850°C

##### 4.3.1. Critical Cr alloy concentration

Oxidation of Fe-20Cr in Ar-5H<sub>2</sub>O-(5H<sub>2</sub>) at 850 °C led to the formation of uniform Cr<sub>2</sub>O<sub>3</sub> scales. Wagner's theory (1) is now used to evaluate the alloy ability to maintain the Cr<sub>2</sub>O<sub>3</sub> scale growth. The values  $k_p = 6.4 \times 10^{-14}$  (Ar-5 H<sub>2</sub>O) and  $1.3 \times 10^{-13} \text{ cm}^2/\text{s}$  (Ar-5H<sub>2</sub>O-5H<sub>2</sub>O) for Fe-20Cr were estimated from (2) using the chromia layer's average thickness after 70 h reactions at 850 °C (Table 3). The  $\tilde{D}_{\text{Cr}} = 1.5 \times 10^{-11} \text{ cm}^2/\text{s}$  value for Fe-20Cr was taken as volume diffusion coefficient from [17] for Fe-12Cr-Mo-V steel ( $\alpha$  phase). The calculated  $N_{\text{Cr}}^{\text{crit}}$  values of 0.04 in

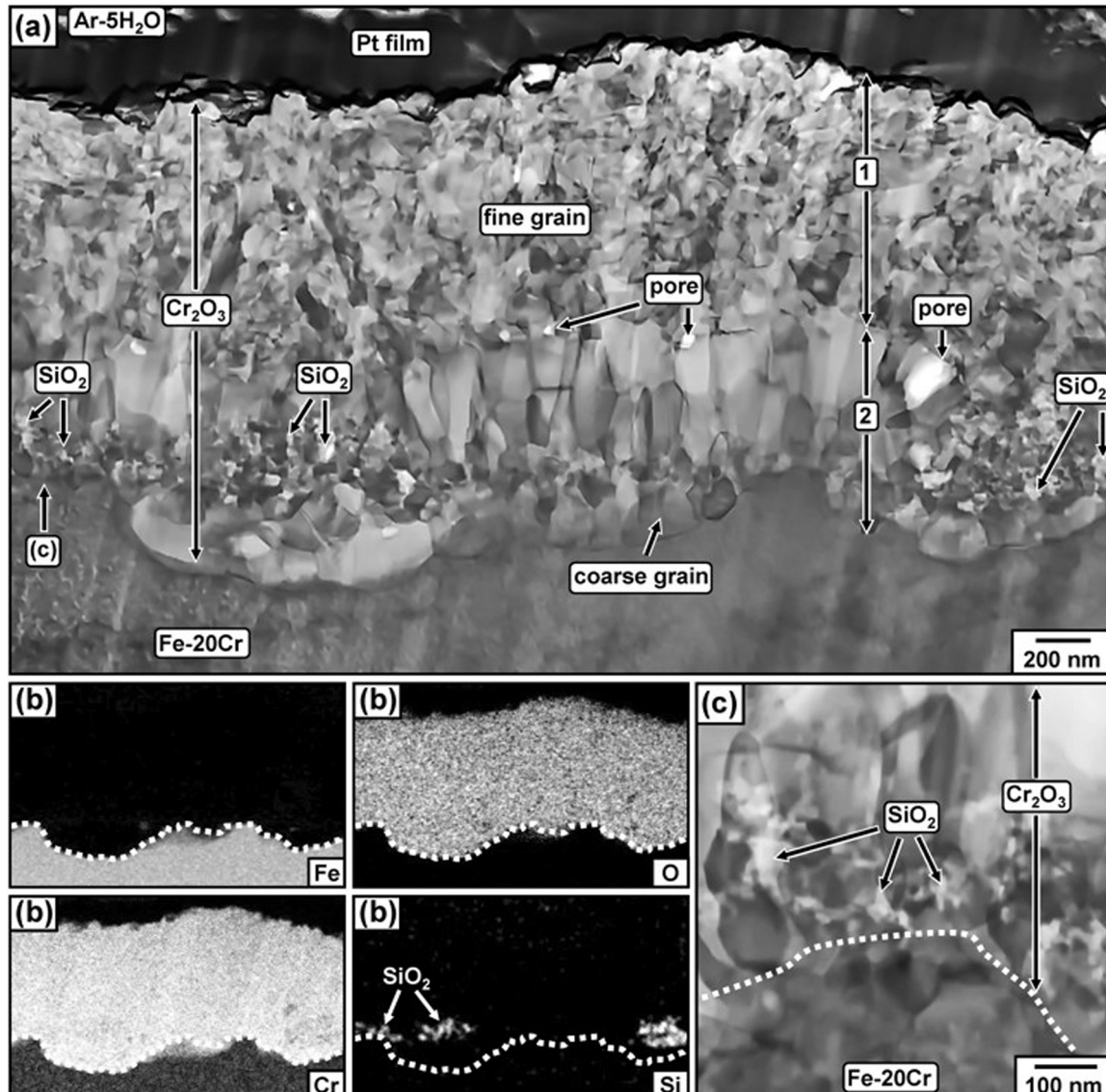


**Fig. 18.** Inert  $\text{SiO}_2$  marker test of Fe-20Cr at 850 °C for 24 h in Ar-5  $\text{H}_2\text{O}$ : (a) BF-STEM cross-section, (b) EDX mapping, and (c) high magnification image of the scale-alloy interface shown in (a).

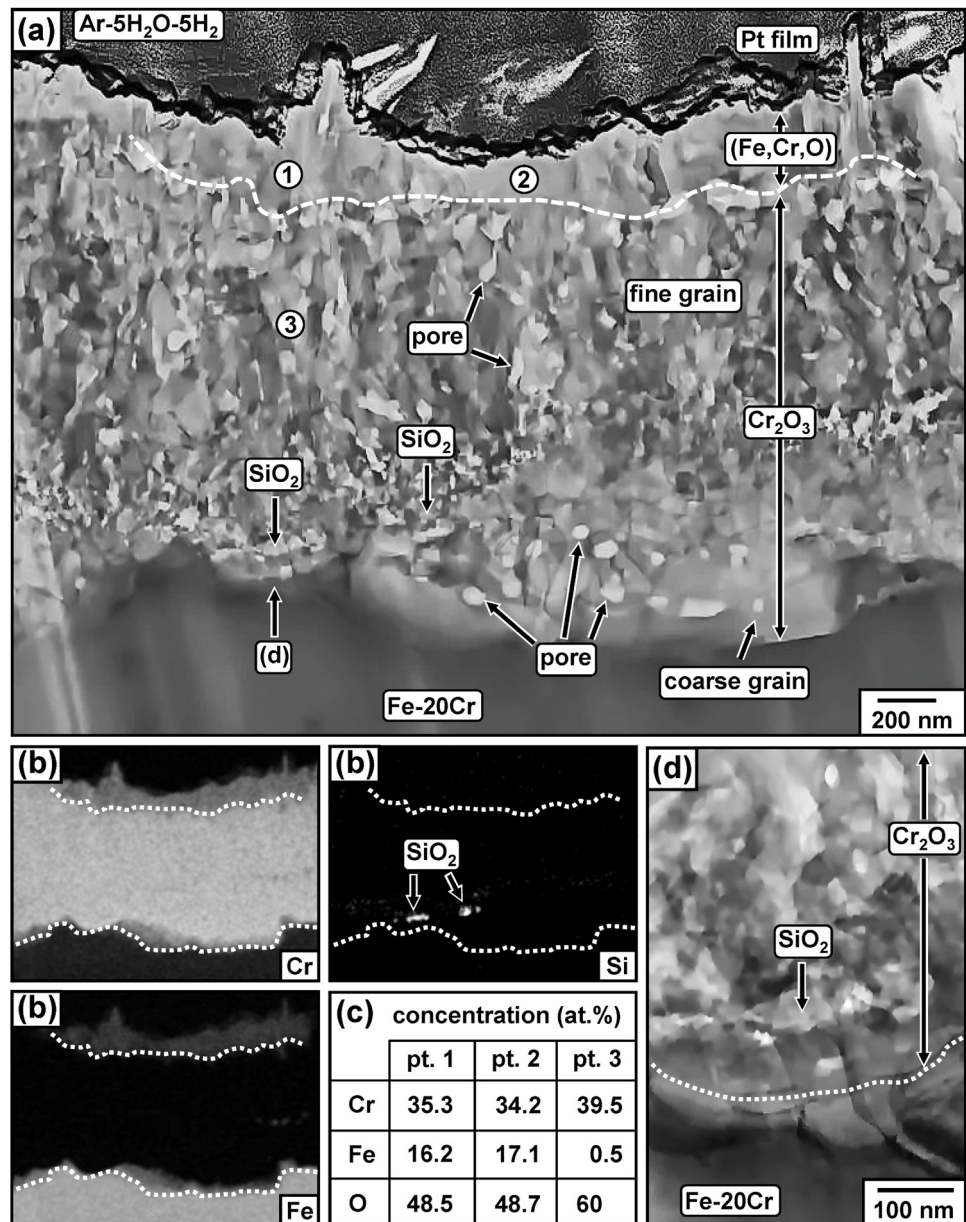


**Fig. 19.** Inert SiO<sub>2</sub> marker test of Fe-20Cr at 850 °C for 24 h in Ar-5 H<sub>2</sub>O-5 H<sub>2</sub>: (a) BF-STEM cross-section, (b) EDX mapping, (c) EDX concentrations of points 1–3 and (d) high magnification image of the scale-alloy interface shown in (a).

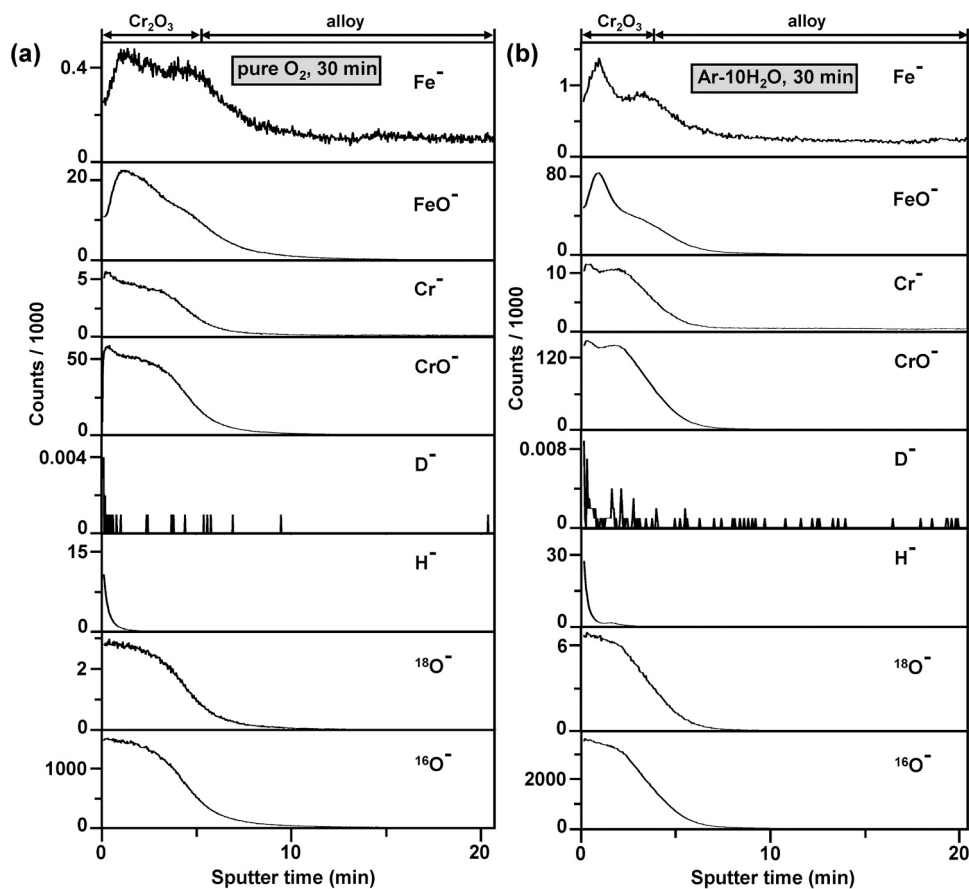


Fig. 20. ToF-SIMS depth profiles of Fe-30Cr oxidized at 650 °C for 30 min in: (a) pure O<sub>2</sub> and (b) Ar-10 H<sub>2</sub>O.

Ar-5H<sub>2</sub>O and 0.06 in Ar-5H<sub>2</sub>O-5H<sub>2</sub> indicates that Fe-20Cr ( $N_{Cr} = 0.21$ ) is able to maintain a Cr<sub>2</sub>O<sub>3</sub> scale in both gases, in agreement with experimental results (Table 3).

#### 4.3.2. Effect of hydrogen on Cr<sub>2</sub>O<sub>3</sub> scale growth in H<sub>2</sub>O at 850 °C

The hydrogen addition to water vapour at 850 °C resulted in

- Smaller Cr<sub>2</sub>O<sub>3</sub> grains (Table 3).
- Faster Cr<sub>2</sub>O<sub>3</sub> scale growth (Table 3).
- Formation of fine pores in the Cr<sub>2</sub>O<sub>3</sub> scale (Figs. 14, 15).

The Cr<sub>2</sub>O<sub>3</sub> scales grown in Ar-5H<sub>2</sub>O-(5H<sub>2</sub>) consisted of mainly columnar grains and some equiaxed grains (Figs. 12, 14, 15), whilst the columnar grains formed in Ar-5H<sub>2</sub>O were wider than those in Ar-5H<sub>2</sub>O-5H<sub>2</sub> (Table 3). The  $k_p$  values calculated from (2) for 70 h reactions are  $k_p = 6.4 \times 10^{-14}$  (Ar-5H<sub>2</sub>O) and  $1.3 \times 10^{-13}$  cm<sup>2</sup>/s (Ar-5H<sub>2</sub>O-5H<sub>2</sub>). The ratio between  $k_p$  values is

$$\frac{k_p^{H_2O}}{k_p^{H_2O-H_2}} = \frac{6.4 \times 10^{-14}}{1.3 \times 10^{-13}} = 0.5 \quad (21)$$

Scaling rate ratios for *p*- and *n*-type Cr<sub>2</sub>O<sub>3</sub> calculated from Eqs. (13), (19) using oxide grain widths  $d = 150$  nm (Ar-5H<sub>2</sub>O) and 130 nm (Ar-5H<sub>2</sub>O-5H<sub>2</sub>) and  $p_{O_2}$  (Table 1) are listed in Table 4. It is clear that the rate ratio predicted for *n*-type Cr<sub>2</sub>O<sub>3</sub> (0.9) is much closer to that calculated by scale thicknesses (0.5) than that expected for *p*-type Cr<sub>2</sub>O<sub>3</sub> (79). Therefore, it is concluded the Cr<sub>2</sub>O<sub>3</sub> scales formed at 850 °C in Ar-5H<sub>2</sub>O-(5H<sub>2</sub>) were not *p*-type, in agreement with previous reports [23,24]. The smaller Cr<sub>2</sub>O<sub>3</sub> grains in H<sub>2</sub>O-H<sub>2</sub> provided more grain boundaries for the outward Cr transport, leading to faster Cr<sub>2</sub>O<sub>3</sub> scale growth rates at both 750 and 850 °C.

The Cr<sub>2</sub>O<sub>3</sub> scale grown in Ar-5H<sub>2</sub>O-5H<sub>2</sub> contained intergranular and intragranular pores (Figs. 14, 15). Because the Cr<sub>2</sub>O<sub>3</sub> scale growth depended mainly on grain boundary diffusion and the volume fraction of pores was small (6 %), the internal pores had little effect on the outward Cr transport through the scale and locations of SiO<sub>2</sub> particles in the scale (Fig. 19).

Further study is needed to understand the role of hydrogen in forming fine pores in the Cr<sub>2</sub>O<sub>3</sub> scale in H<sub>2</sub>O-H<sub>2</sub> and their possible effects on scaling.

#### 4.4. Transport of hydrogen in Cr<sub>2</sub>O<sub>3</sub> scale during oxidation in water vapour

The ToF-SIMS depth profiles of Fe-30Cr oxidized in Ar-10D<sub>2</sub>O (Fig. 21) and a two-stage experiment (Fig. 22) show enrichments of deuterium at the outermost Cr<sub>2</sub>O<sub>3</sub> scale surface and near the scale-alloy interface. Clearly, D-bearing species entered the Cr<sub>2</sub>O<sub>3</sub> scale during reactions in Ar-10D<sub>2</sub>O. Furthermore, the two-stage experiment demonstrated that deuterium from D<sub>2</sub>O diffused through the scale preformed in H<sub>2</sub>O. Whilst this supports the hypothesis that some water-vapour-derived species enters chromia grain boundaries, further study is needed to determine the chemical forms of such species enriched in the Cr<sub>2</sub>O<sub>3</sub> scale.

Liquid water and atmospheric oxygen contain a small amount of isotope <sup>18</sup>O, with an <sup>18</sup>O abundance of about 0.2 atom % [27]. The signal intensity ratio of <sup>18</sup>O/<sup>16</sup>O in the scales after exposures to O<sub>2</sub> and H<sub>2</sub>O (Fig. 20) was about 0.2 % and 0.3 % for D<sub>2</sub>O (Fig. 21b). Clearly, the detection of <sup>18</sup>O by ToF-SIMS analysis is expected and reflects the natural abundance ratio for the oxygen isotopes. Permeability of hydrogen through a chromia scale at 1000 °C in a low oxygen gas is available in [28].

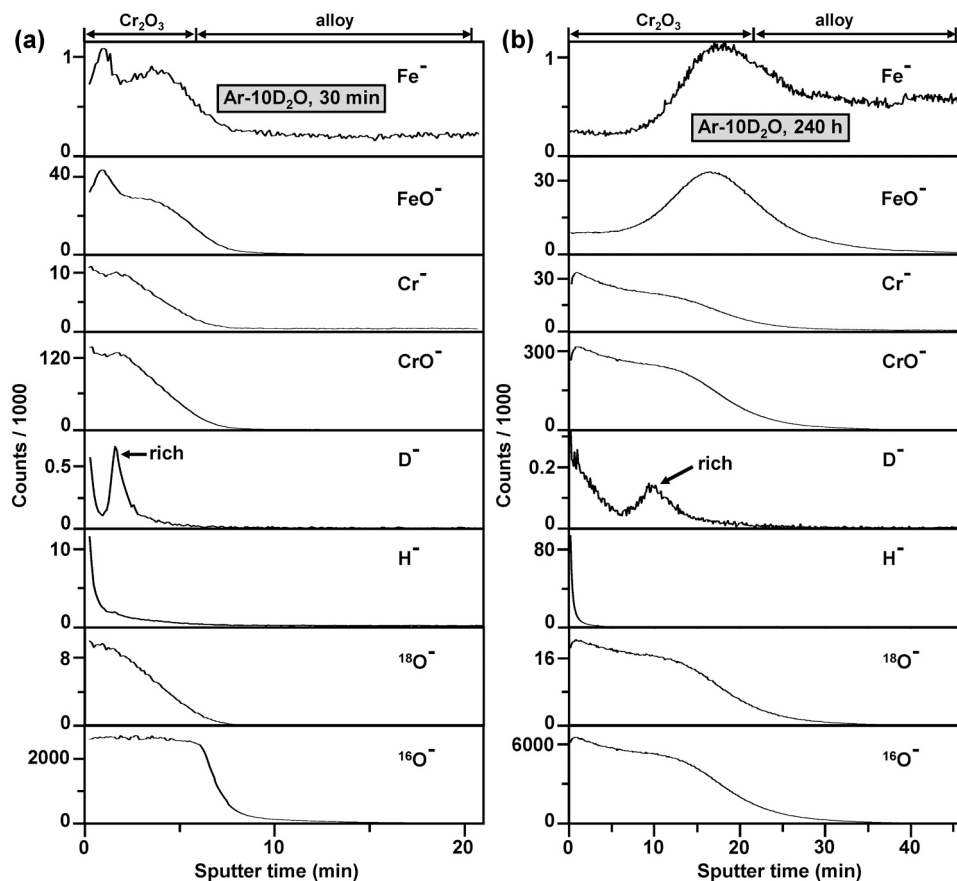


**Fig. 21.** ToF-SIMS depth profiles of Fe-30Cr oxidized at 650 °C in Ar-10D<sub>2</sub>O for: (a) 30 min (ion sputter current: 35.5 nA) and (b) 240 h (ion sputter current: 69 nA).

## 5. Conclusions

The model Fe-20Cr alloy formed a uniform Cr<sub>2</sub>O<sub>3</sub> scale in Ar-200<sub>2</sub> but a mixture of Cr<sub>2</sub>O<sub>3</sub> and Fe-rich oxides in Ar-20H<sub>2</sub>O-(5H<sub>2</sub>) at 750 °C. Wagner's theory shows that in general the alloy Cr concentration was enough to maintain the growth of Cr<sub>2</sub>O<sub>3</sub> scales, but not for local, fast growing Cr<sub>2</sub>O<sub>3</sub> scales. Consequent alloy depletion in Cr was concluded to be the cause of breakaway oxidation and Fe-rich oxide nodule formation at 750 °C in Ar-20H<sub>2</sub>O.

The Fe-20Cr alloy formed protective Cr<sub>2</sub>O<sub>3</sub> scales in Ar-5H<sub>2</sub>O-(5H<sub>2</sub>) at 850 °C, as a result of faster alloy Cr diffusion at this temperature. The Cr<sub>2</sub>O<sub>3</sub> scale formed in Ar-5H<sub>2</sub>O was dense, but that in Ar-5H<sub>2</sub>O-5H<sub>2</sub> contained numerous pores. The pores are very fine (~ 0.1 μm) and could contribute to grain refinement, but the mechanism of their formation is as yet unknown.

The two-stage experiment at 750 °C and inert SiO<sub>2</sub> marker tests at 850 °C indicated that Cr<sub>2</sub>O<sub>3</sub> scale growth was controlled mainly by outward Cr diffusion in H<sub>2</sub>O-(H<sub>2</sub>). Addition of H<sub>2</sub> to water vapour resulted in smaller Cr<sub>2</sub>O<sub>3</sub> grains and faster Cr<sub>2</sub>O<sub>3</sub> scale growth at both 750 and 850 °C.

Wagner's theory was successful in identifying effects of grain sizes and oxygen partial pressures of gases on scale growth rates, showing a predominant role of grain boundary transport. The Cr<sub>2</sub>O<sub>3</sub> scales formed in H<sub>2</sub>O and H<sub>2</sub>O-H<sub>2</sub> at both temperatures were not p-type.

Transport of deuterium through a Cr<sub>2</sub>O<sub>3</sub> scale during oxidation of Fe-30Cr in Ar-10D<sub>2</sub>O was confirmed by ToF-SIMS analysis. An enrichment of deuterium was observed in the scale near the scale-alloy interface. On this basis, it is concluded that water vapour-derived species entered chromia grain boundaries and affected their diffusion properties.

## Author statement

I, the Corresponding Author, declare that this manuscript is original, has not been published before and is not currently being considered for publication elsewhere. I can confirm that the manuscript has been read and approved by all named authors and that there are no other persons who satisfied the criteria for authorship but are not listed. I further confirm that the order of authors listed in the manuscript has been approved by all of us. I understand that the Corresponding Author is the sole contact for the Editorial process and is responsible for communicating with the other authors about progress, submissions of revisions and final approval of proofs.

## CRediT authorship contribution statement

**David J. Young:** Writing – review & editing, Supervision, Project administration, Investigation, Funding acquisition. **Thuan Dinh Nguyen:** Writing – original draft, Visualization, Methodology, Investigation, Formal analysis, Data curation, Conceptualization. **Jianqiang Zhang:** Writing – review & editing, Supervision, Project administration, Funding acquisition, Conceptualization.

## Declaration of Competing Interest

The authors declare the following financial interests/personal relationships which may be considered as potential competing interests: Jianqiang Zhang, David J. Young reports financial support was provided by Australian Research Council. If there are other authors, they declare that they have no known competing financial interests or personal relationships that could have appeared to influence the work reported in this paper.

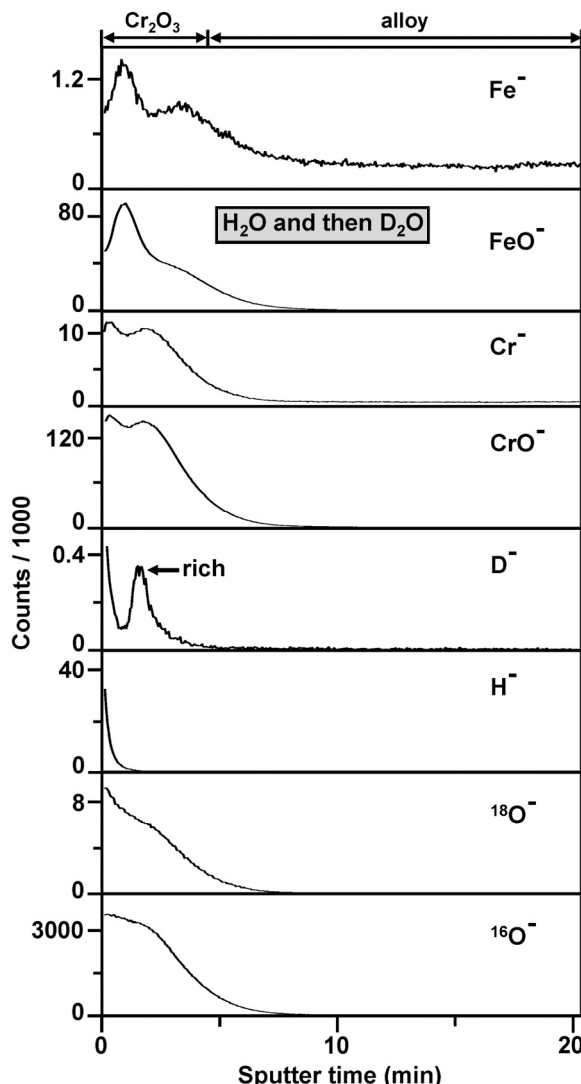


**Fig. 22.** ToF-SIMS depth profiles of Fe-30Cr oxidized at 650 °C in 2 stages: 30 min in Ar-10 H<sub>2</sub>O and then 30 min in Ar-10D<sub>2</sub>O (ion sputter current: 71.4 nA).

**Table 4**  
Chromia scale growth rate ratios at 750 and 850 °C.

Rate ratio	750 °C	850 °C
$\frac{k_p^{\text{H}_2\text{O}}}{k_p^{\text{H}_2\text{O}-\text{H}_2}}$ from measured X values	0.3	0.5
$\frac{k_p^{\text{H}_2\text{O}}}{k_p^{\text{H}_2\text{O}-\text{H}_2}}$ predicted, p-type Cr <sub>2</sub> O <sub>3</sub>	65	79
$\frac{k_p^{\text{H}_2\text{O}}}{k_p^{\text{H}_2\text{O}-\text{H}_2}}$ predicted, n-type Cr <sub>2</sub> O <sub>3</sub>	0.5	0.9

## Data Availability

Data will be made available on request.

## Acknowledgement

Financial support from the Australian Research Council's Discovery Program (DP220102392) is gratefully acknowledged.

## References

- [1] B. Pujilaksono, T. Jonsson, H. Heidari, M. Halvarsson, J.-E. Svensson, L.-G. Johansson, Oxidation of binary FeCr alloys (Fe-2.25Cr, Fe-10Cr, Fe-18Cr and Fe-25Cr) in O<sub>2</sub> and in O<sub>2</sub> + H<sub>2</sub>O Environment at 600 °C, *Oxid. Met.* 75 (2011) 183–207.
- [2] N. Mu, K. Jung, N.M. Yanar, F.S. Pettit, G.R. Holcomb, B.H. Howard, G.H. Meier, The effects of water vapor and hydrogen on the high-temperature oxidation of alloys, *Oxid. Met.* 79 (2013) 461–472.
- [3] N.K. Othman, J. Zhang, D.J. Young, Water vapour effects on Fe-Cr alloy oxidation, *Oxid. Met.* 73 (2010) 337–352.
- [4] M. Schütze, D. Renusch, M. Schorr, Parameters determining the breakaway oxidation behaviour of ferritic martensitic 9%Cr steels in environments containing H<sub>2</sub>O, *Corros. Eng. Sci. Technol.* 39 (2004) 157–166.
- [5] E. Essuman, G.H. Meier, J. Zurek, M. Hansel, W.J. Quadakkers, The effect of water vapor on selective oxidation of Fe-Cr alloys, *Oxid. Met.* 69 (2008) 143–162.
- [6] C.T. Fujii, R.A. Meissner, Oxide structures produced on iron-chromium alloys by a dissociative mechanism, *J. Electrochem. Soc.* 110 (1963) 1195–1204.
- [7] H. Hooshyar, T. Jonsson, J. Hall, J.-E. Svensson, L.G. Johansson, J. Liske, The effect of H<sub>2</sub> and H<sub>2</sub>O on the oxidation of 304L stainless steel at 600 °C: general behaviour (Part I), *Oxid. Met.* 85 (2016) 321–342.
- [8] D.J. Young, J. Zurek, L. Singheiser, W.J. Quadakkers, Temperature dependence of oxide scale formation on high-Cr ferritic steels in Ar-H<sub>2</sub>-H<sub>2</sub>O, *Corros. Sci.* 53 (2011) 2131–2141.
- [9] A. Vayala, I. Povstugar, T. Galiullin, D. Naumenko, W.J. Quadakkers, H. Hattendorf, J. Mayer, Effect of Nb addition on oxidation mechanisms of high Cr ferritic steel in Ar-H<sub>2</sub>-H<sub>2</sub>O, *Oxid. Met.* 92 (2019) 471–491.
- [10] M. Hänsel, W.J. Quadakkers, D.J. Young, Role of water vapor in chromia-scale growth at low oxygen partial pressure, *Oxid. Met.* 59 (2003) 285–301.
- [11] FactSage 8.1. Database: FactPS.
- [12] K.F. McCarty, D.R. Boehme, A Raman study of the systems Fe<sub>3-x</sub>Cr<sub>x</sub>O<sub>4</sub> and Fe<sub>2-x</sub>Cr<sub>x</sub>O<sub>3</sub>, *J. Solid State Chem.* 79 (1989) 19–27.
- [13] D.L.A. de Faria, S. Venancio Silva, M.T. de Oliveira, Raman microspectroscopy of some iron oxides and oxyhydroxides, *J. Raman Spectrosc.* 28 (1997) 873–878.
- [14] T.D. Nguyen, J. Zhang, D.J. Young, Silicon contamination during alloy oxidation in water vapour at 650 °C, *Oxid. Met.* 97 (2022) 559–574.
- [15] T.D. Nguyen, J. Zhang, D.J. Young, Effect of volatile silicon species on chromia scale microstructures, *Corros. Sci.* 209 (2022) 110808.
- [16] C. Wagner, Theoretical analysis of the diffusion processes determining the oxidation rate of alloys, *J. Electrochem. Soc.* 99 (1952) 369–380.
- [17] Z. Tökei, K. Hennesen, H. Viehhaus, H.J. Grabke, Diffusion of chromium in ferritic and austenitic 9–20 wt% chromium steels, *Mater. Sci. Technol.* 16 (2000) 1129–1138.
- [18] D.J. Young, B.A. Pint, Chromium volatilization rates from Cr<sub>2</sub>O<sub>3</sub> scales into flowing gases containing water vapour, *Oxid. Met.* 66 (2006) 137–153.
- [19] C. Wagner, Beitrag zur Theorie des Anlaufvorgangs, *Z. Phys. Chem.* 21 (1933) 25–41.
- [20] D.J. Young, High Temperature. Oxidation and Corrosion of Metals, first ed., Elsevier, UK, 2008 page 485.
- [21] D. Caplan, G.I. Sproule, Effect of oxide grain structure on the high-temperature oxidation of Cr, *Oxid. Met.* 9 (1975) 459–472.
- [22] R.J. Hussey, D.F. Mitchell, M.J. Graham, The growth and structure of oxide films formed on single crystal (100) and polycrystalline Cr between 550 and 900°C, *Mater. Corros.* 38 (1987) 575–583.
- [23] L. Latu-Romain, Y. Parsa, S. Mathieu, M. Vilasi, A. Galerie, Y. Wouters, Towards the growth of stoichiometric chromia on pure chromium by the control of temperature and oxygen partial pressure, *Corros. Sci.* 126 (2017) 238–246.
- [24] X. Huang, L. Martinelli, S. Bosonnet, P.C.M. Fossati, L. Latu-Romain, Y. Wouters, Effect of temperature on the oxidation mechanism of Ni-30Cr alloy, *Oxid. Met.* 96 (2021) 69–80.
- [25] E.N. Bunting, Phase equilibria in the system Cr<sub>2</sub>O<sub>3</sub>-SiO<sub>2</sub>, *J. Res. Natl. Bur. Stand.* (1930) 325–327.
- [26] G. Bamba, Y. Wouters, A. Galerie, G. Borchardt, S. Shimada, O. Heintz, S. Chevalier, Inverse growth transport in thermal chromia scales on Fe-15Cr steels in oxygen and in water vapour and its effect on scale adhesion, *Scr. Mater.* 57 (2007) 671–674.
- [27] W. Dansgaard, The O<sub>18</sub>-abundance in fresh water, *Geochim. Cosmochim. Acta* 6 (1954) 241–260.
- [28] M. Tanaka, M. Ueda, K. Kawamura, T. Maruyama, Hydrogen permeability through n-type Cr<sub>2</sub>O<sub>3</sub> scale at 1273 K under the oxygen activities of  $1.6 \times 10^{-18}$  –  $1.0 \times 10^{-16}$ , *ISIJ Int.* 51 (2011) 638–644.